

ЭМС В УСЛОВИЯХ ВОЗДЕЙСТВИЯ ПРИРОДНЫХ ЯВЛЕНИЙ

NATURAL NOISE SOURCES

M. HAYAKAWA¹, Y. FUKUMOTO¹, AND H. YASUDA²

1. Department of Electronic Engineering, The University of Electro-Communications, 1-5-1 Chofugaoka, Chofu Tokyo 182-8585, Japan

2. Taiyo Musen Co., Ltd., Ebisu-nishi 2-20-7, Shibuya, Tokyo, Japan

RECEPTION OF OVER-HORIZON FM TRANSMITTER SIGNALS ASSOCIATED WITH EARTHQUAKES

Abstract Over-horizon FM signal is received on abnormal situations (probably in close association with earthquakes). This paper presents our latest results on the characteristics of such over-horizon signals on the basis of the measurements by different antenna systems (transmitter: FM Sendai (77.1 MHz) and receiving station: Chofu). First of all, the reception of over-horizon signal is cross-correlated with the earthquake, and it is found that such signals are mainly observed about 7 days before an earthquake. Then, such signals are found to have small elevation signal ($\sim 10^\circ$), which implies that the signal is due to tropospheric effect (not ionospheric scattering). Signal bearings are estimated by direction finding, but the signal bearing is always considerably different from the future epicentral direction (always close to the coastal region). Finally, the signal intensity is significantly large (far from the level of scattered signal), so that the signal reception is probably due to the favorable VHF tropospheric condition attributed to the effect of earthquakes.

1. Introduction

Electromagnetic phenomena are recently considered to be very promising for the short-term earthquake prediction [Hayakawa and Fujinawa, 1994; Hayakawa, 1999]. One of the electromagnetic sounding is the use of pre-existing transmitter signals in different frequency ranges to study the seismo-atmospheric and -ionospheric phenomena. Rather convincing results on the seismo-ionospheric perturbations have been reported in VLF and LF band [Gokhberg et al., 1989; Hayakawa et al., 1996; Molchanov and Hayakawa, 1989]. Also, Biagi et al. [1999] have investigated the seismo-atmospheric effect in the subionospheric LF(150-300kHz) wave propagation.

In VHF frequency range, Kushida (personal communication, 2000) have been working on the reception of over-horizon FM transmitter signals which, he considers, is associated with earthquakes and his considers

such a reception of the over-horizon VHF signal being due to ionospheric scattering. However, its mechanism is extremely poorly understood, so that we will present our latest results in order to answer the fundamental questions including, (1) can we receive an over-horizon FM transmitter signal before an earthquake? and (2) what is the mechanism of such a reception of over-horizon FM signals associated with earthquakes?

2. Observation, receiving and antenna systems

Fig. 1 illustrates the relative location of the FM transmitter in Sendai (frequency = 77.1 MHz, power = 5 kW, height = 193 m, and horizontal polarization) and the receiver at our university (UEC) (antenna height=33.8m). The distance between the transmitter and receiver is 312km and the line of sight is 80km. Crosses in the figure indicate the epicenters of earthquakes with magnitude greater than 3.5 during our period

of observation. The period of our observation is February 1st through June 30, 2000, in which the midnight (L.T.=0:00-5:30h) data are used because during other time periods the radio broadcasting (University of the Air) is going on at this same frequency in Tokyo area.

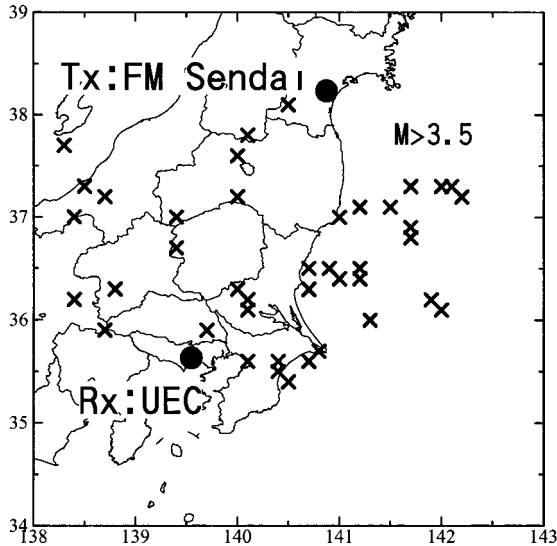


Fig. 1 Relative location of the FM transmitter in Sendai and the receiving station (our university).

The receiver system is composed of a HF amplifier, a mixer with an oscillator, an IF amplifier and a detector (to detect low frequency component). In this study we record the IF signal and the sampling is 0.1Hz.

We next describe the antenna systems. 6 Yagi antenna systems are used (each Yagi has 5 elements). As for the horizontal polarization, we have three different bearing (azimuthal) angles of -30° , 0° , $+30^\circ$ (0° means the direction between the receiver and transmitter; - indicates the west of the path and + means the east of the path) for the elevation angle= 0° (horizontal), and these antenna systems for horizontal polarization with three different elevation angles (0° , 45° , and 90° (vertical upward)) for the fixed azimuth of 0° . Additionally, we have one antenna with vertical polarization (bearing= 0° , elevation= 0°). By using the outputs from the two antennas (S(+) and S(-)) (bearing= $+30^\circ$ and -30° , respectively), we can estimate the azimuth of the observed signal by using the relationship of $\Theta = \tan^{-1}(S(+)/S(-))$ and also the

absolute amplitude (because the system is well calibrated).

3. Observed results and correlation analysis

On the normal days without any effect of earthquakes, we observe the background levels for all of six antenna channels. However, when a certain effect (probably the effect of an earthquake) happens, we have the record such as on May 27, 2000 as shown in Fig. 2. Looking at the three panels (top right two and bottom left) directed to three different bearings (but with the same horizontal polarization and the same elevation angle= 0°), the most significant output is seen for the azimuth $+30^\circ$ (east of the path). By using the output from the two antennas (S(+) and S(-)) we can perform the direction finding, which has indicated that the over-horizon signal is found to have the bearing of about $+20^\circ$ (east of the path). Next, we discuss the incident angle of the signal by looking at the bottom three panels. As is easily seen from the panels, the output for the elevation= 0° is strongest, next for elevation= 45° , and a negligible output is seen for elevation= 90° (vertical upward). By taking into account the radiation pattern in the elevation direction, the incident angle is estimated to be $\sim 10^\circ$. It is furthermore confirmed that the sound signal of the observed FM wave is the one from FM Sendai, so that we are receiving the over-horizon signal of FM Sendai. It is uncertain here that this abnormal reception of the over-horizon signal is a precursor to any earthquakes, because there were a few earthquakes after this signal.

In order to study the possible correlation between such an anomalous reception (as in Fig. 2) and any earthquake, we perform the cross-correlation analysis. First, we deal with the earthquakes (total number is about 30) taking place in the east of the path (occurring within a radius of 300km from the receiver with azimuth less than 120°) with magnitude greater than 3.5. We take an average of the signal amplitude during one particular day as one variable $x(t)$ (t: time; day) and another variable $y(t)$ characterizes the earthquake in the following manner (y:

$(\exp(11.8+1.5M)/d) \times (1/r)$ (M: magnitude, d: depth, r: epicentral distance), based on the reasonable assumption that the signal intensity is proportional to the energy released during an earthquake and also is closely related with d and r in such a way. When we have a few earthquakes on the same day, we adopt the largest value for $y(t)$. The cross-correlation result, which is the result for the earthquakes taking place in the east of the path, is given. We find that there exists a sig-

nificant peak around -7 days; which means that the anomalous reception of over-horizon FM signal is received mainly about 7 days before the quake.

The same analysis was performed for the earthquakes taking place in the west of the path, but the result is not reliable (and also not shown here) because the number of events is extremely small as compared with those in the east of the path.

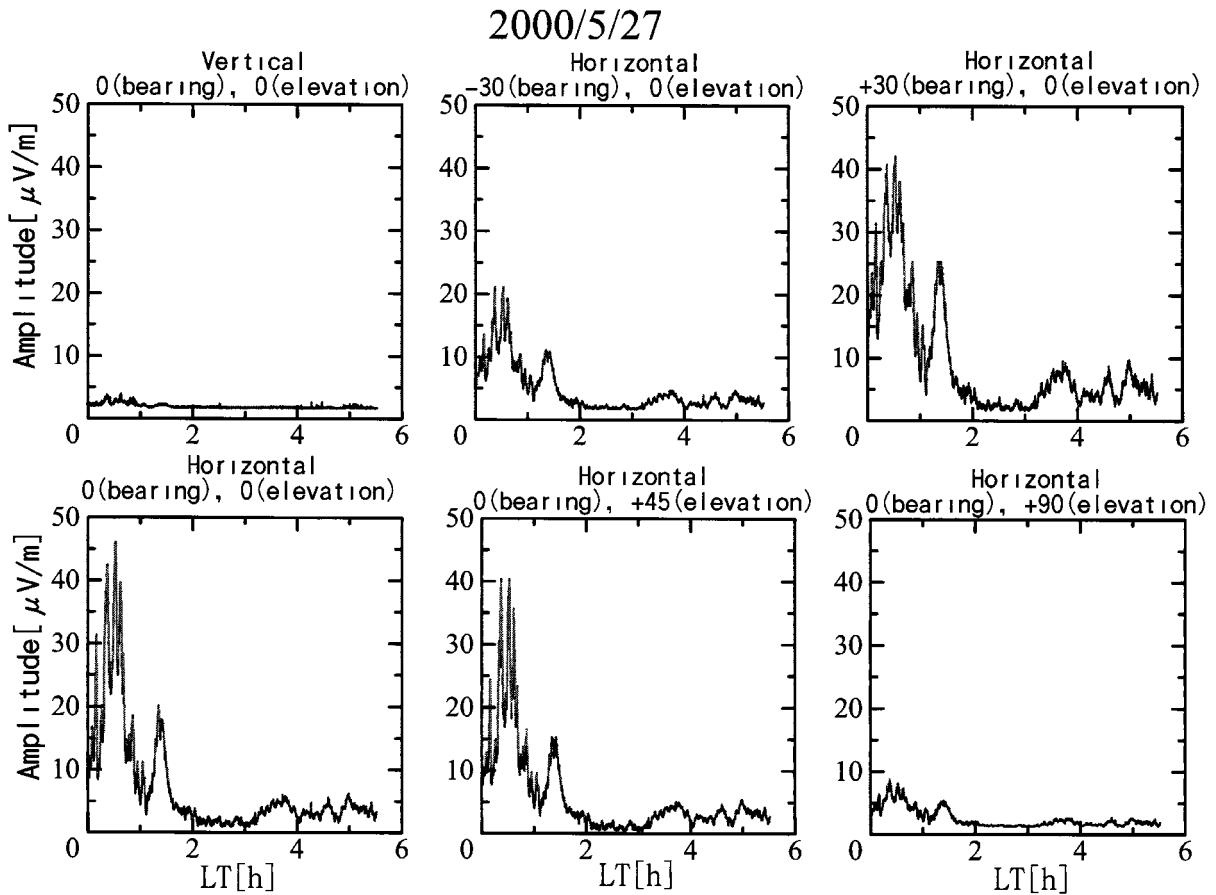


Fig. 2 An example of abnormal reception of over-horizon FM signal on May 27, 2000. The outputs from six different antenna systems are illustrated; from left to right on the upper panel; (1) vertical polarization (bearing=0°, elevation=0°), (2) horizontal polarization (bearing=-30°, elevation=0°), (3) same polarization (bearing+30°, elevation=0°), then on the lower panel, from right to left; (4) horizontal polarization (bearing=0°, elevation=0°) (5) same polarization (bearing=0°, elevation=45°) and (6) same polarization (bearing=0°, elevation=90°(upward)).

If we consider this time delay of approximate 7 days as the maximum cross-correlation and we apply this to the data observed in Fig. 2, the abnormal signal on May 27 in Fig. 2 is likely to be a precursor of a big earthquake (M=5.8) occurred on June 3, whose azimuth is +94°. However, the direc-

tion finding gives us the result of +20° for the event in Fig. 2, and there seems to be a significant difference between the observed signal bearing and epicentral direction. The statistical analysis on such a difference between the signal bearing and the corresponding epicentral direction is summarized, indicating

that the signal bearing is always more westward than the epicentral direction (the maximum difference is peaked at $\sim 30^\circ$). We suggest that the signal is coming very close to the coast of Japan Islands. This may be due to a large perturbed region due to the earthquake. Next, we comment on the statistical result on the signal elevation, which indicates that signal elevation is less than 20° , with peaking at about 10° .

Fig. 3 illustrates the intensity of the observed over-horizon FM signal, to be compared with the theoretical expectation. The full line is the theoretical curve for the expected signal amplitude based on the information on the transmitter characteristics (antenna power etc.) and receiver height. Up to the distance of line of sight (~ 50 - 80 km), the wave is space wave and beyond this critical distance we have only the diffracted wave. The observed signal intensity is mainly at the free space intensity or a little lower than it. So that we can conclude that the free-space wave is reflected by some irregularity in the troposphere.

4. Conclusion and discussion

The following observational facts have emerged from the present analysis during six months.

(1) An over-horizon FM transmitter signals (though it is not received on normal conditions) is sometime observed on abnormal conditions (probably associated with earthquakes).

(2) Such abnormal over-horizon FM signals are found to be received at our observing station with small incident angle (incident angle $< 20^\circ$).

(3) The direction finding of the bearing of observed over-horizon signal shows that there is sometime a lot of difference with regards to the bearing of the future epicenter.

(4) The cross-correlation between the abnormal over-horizon FM signal and earthquakes, indicates that there is a significant peak around 7 days before the quake. It seems that over-horizon abnormal signals are observed about 7 days before the quake.

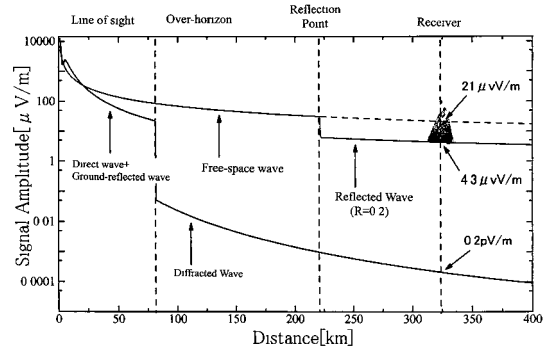


Fig. 3 Theoretical estimation of signal intensity as a function of distance, together with the observed signal intensity.

Based on these observational facts, we try to answer the fundamental questions raised in the Introduction. First of all, the signal from FM Sendai is really observed on some occasions at the receiving station beyond the horizon. On the basis of the cross-correlation between the reception of over-horizon FM signal and earthquakes, those over-horizon signals are found to be positively correlated with an earthquake, with a significant time delay of around 7 days, and hence it is highly likely that such reception is due to the effect of earthquakes. Those over-horizon signals are observed with small elevation angle (around 10° , and less than 20°), which may imply that signal reception is due to tropospheric effect (definitely not due to ionospheric scattering). Also, the signal bearing of the observed signal is significantly different from the future epicentral direction, and we may infer that the perturbed region is considerably large (with radius of 100km based on the consideration of the signal bearing and epicentral position) and the signal is likely to be coming from the coastal region. And their important point is that the signal intensity is much higher than the diffracted level and significantly large as shown in Fig. 5. So, this means that the signal reception is unlikely to be due to the tropospheric scattering, but due to very favorable tropospheric propagation condition associated with an earthquake (this mechanism should be considered in future).

Additionally we comment on the natural noise using the vertical polarization. This suggests that the natural noise in VHF may be generated in close association with earth-

quakes, but we need more data for the definite conclusion.

City University for his assistance in system design.

Acknowledgement

The author would like to express their sincere thanks to T. Yoshida of Hiroshima

References

Hayakawa, M., Editor, Atmospheric and Ionspheric Electromagnetic Phenomena Associated with Earthquakes, Terra Sci. Pub. Co., 997p, Tokyo, 1999.

*A. P. NICKOLAENKO¹, L. M. RABINOWICZ¹, AND A. V. SHVETS¹,
A. YU. SCHEKOTOV², O.A. MOLCHANOV³*

¹Usikov Institute for Radio-Physics and Electronics of the National Academy of Sciences of the Ukraine

²Institute for Terrestrial Magnetism Ionosphere and Radio Propagation (IZMIRAN) of the Russian Academy of Sciences

³National Space Developments Agency of Japan

RESULTS OF R/S ANALYSIS OF THE NATURAL ELF DATA

Abstract. We apply the R/S analysis and evaluate the Hurst exponent of the natural electromagnetic radio signal in the extremely low frequency (ELF) band. We compare the results obtained with natural ELF radio noise recorded in a seismo-active and in a quiet region.

Qualities of natural stochastic signals reflect their origin. The R/S analyses resolves the signals by establishing their statistical structure (*Turcotte, 1997*). The procedure is formally introduces as follows. Let us have a random series of data: $x(t_K) = x_K$, where $K \in [1; N]$ and $N = 2^L$. We divide the initial data series in two parts $M = N/2$ and compute the range R_I and the standard deviation S_I for each part of the record. These functions involved are defined for a given data set in the standard way:

$$R_M = x_{MAX} - x_{MIN} \quad (1),$$

$$S_M = \sqrt{\frac{1}{M-1} \sum_{K=1}^M (x_K - \langle x_M \rangle)^2} \quad (2).$$

and

$$\langle x_M \rangle = \frac{1}{M} \sum_{K=1}^M x_K \quad (3).$$

Then, we find the average R/S ratio:

$$Z(M) = \left\langle \frac{R_I}{S_I} \right\rangle \quad (4)$$

Here, the angular brackets denote averaging over the ensemble.

Then, we brake the series into four parts, obtaining a new length of data sets $M = N/4$. The computational procedure is repeated resulting in a new average value $Z(N/4)$. Then, the procedure is repeated for $M = N/8$, etc. Finally, the elementary segment of data contains only two elements, and parameters R and S satisfy the condition: $R_I = \sqrt{2} \cdot S_I$ so that the 'limiting' or initial value of the R/S ratio is a constant $Z(2) = \sqrt{2}$.

Since the Hurst exponent equals by the definition $Z(M) = (M)^{Hu}$, we plot the logarithm of computed R/S ratio $\log_2(Z)$ against the argument $I = \log_2(M) \in [1, N/2]$, and the

tilt of the best fit straight line gives the value of the Hurst exponent.

Performing the R/S analysis allows us to define the nature of ‘randomness’ present in the statistical data set. For example, when we treat the Gaussian noise, the tilt of the plot equals 0.5. When the normal process is of short duration, its exponent $Hu \rightarrow 1$. So, the R/S curve of a normal noise has the higher tilts first, which are then reduced to the 0.5 stationary value.

The line of 0.5 tilt is of special importance. It divides the noises of two types:

When $Hu \in [0.5; 1.0]$, one speaks that the process contains persistence. This means that the current value of the random variable depends on previous ones (on the process pre-history).

When $Hu \in [0; 0.5]$, we regard the process as anti-persistent one (having no ‘memory’).

Correspondingly, a process is regarded as a persistent one when its $Z(M)$ curve is found above the \sqrt{M} dependence, and it is called the anti-persistent process when this curve lies below the \sqrt{M} line. For the most of natural processes the tilt of the R/S curve corresponds to $Hu \in [0.7; 0.8]$.

We process the ELF signals recorded in a seismo-active region with three orthogonal magnetic antennas working in the frequency range from 0.01 to 20 Hz and compare the data with those collected by Dr. C. Price group at the observatory Mitzpe Ramon of Tel Aviv University placed in the Negev desert, (see *Nickolaenko, Price, Iudin, 2000*).

Figure 1 surveys the results for the monthly data collected in a seismically quiet Negev Desert region. Here, we depict the dynamics of the R/S curves within the interval $I \in [6; 12]$, where the Hurst exponent equals approximately 0.25. Anti-persistence of ELF radio noise proves that individual lightning strokes responsible for the formation of natural signal are completely independent. The left panel in Fig. 1 presents the NS magnetic field, and the right frame shows its EW component. Universal time and days in March 1998 are shown along the vertical axes on the

linear scale. Reciprocity of the survey to individual R/S plots is demonstrated by the terminating plot inserted below the right panel. One may see from the figure that fluctuations of $\text{Log}\langle Z \rangle$ amplitude are approximately proportional to the level $I = \text{Log}\langle M \rangle$. The plots tend to vary as a whole, moving together to higher or lower position with the time. Thick solid curve in Fig.1 represents the smoothed temporal variations of the level $\text{Log}\langle Z(1024) \rangle$. These data were additionally smoothed using 3 points preceding and 3 points following a specific time. Figure 1 demonstrates, that small regular diurnal variations may be found in a quiet field-site conditioned probably by changes in the global thunderstorm activity.

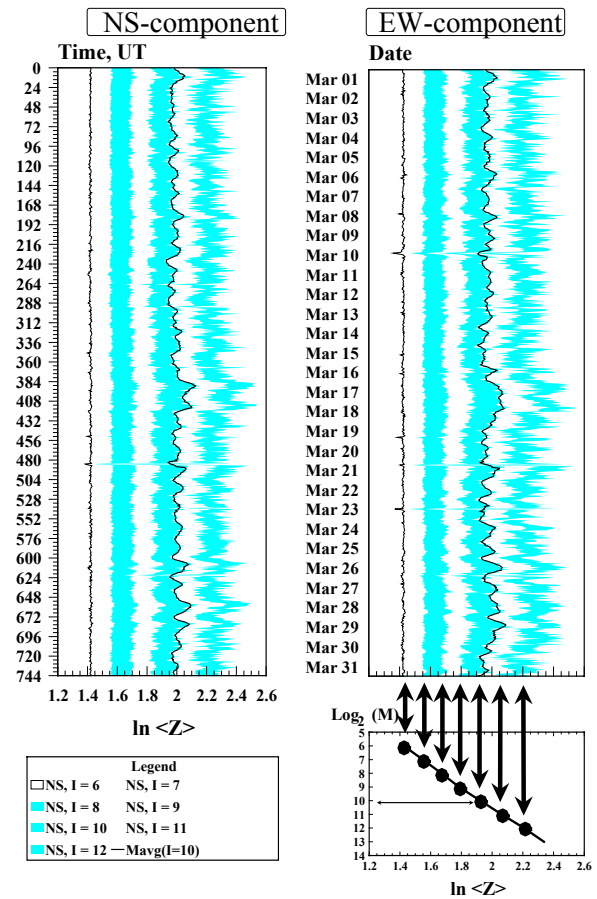


Fig. 1. Monthly dynamics of the R/S curves in a quiet region.

We show in Fig. 2 the results for one day data analyses performed for the three component records of geomagnetic field (components H, D, and Z) at the Karymshino field site (Kamchatka). In general, the curves ob-

tained there were similar to the records obtained in the quiet place (the Negev Desert).

The same inertia interval is observed where the Hurst exponent is close to 0.25 value. Simultaneously, some abrupt modifications of the R/S curves are present in the

records. We see such alterations around 4-7 hr UT in Fig. 2. Separate frames to the right of the main plot demonstrate specific dependencies pertinent to individual field components at particular segments of the record.

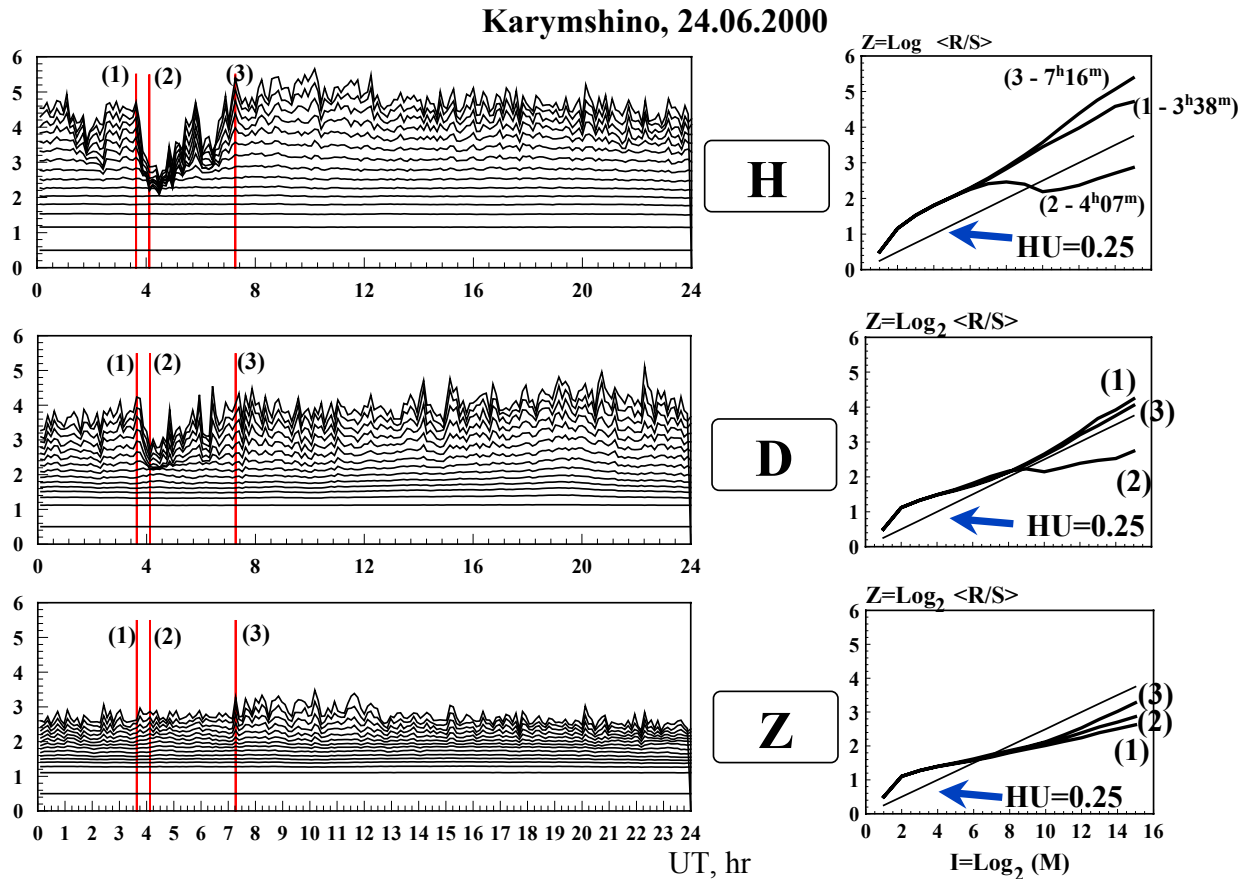


Fig. 2. Dynamics of the R/S curves at seismo-active region.

Each frame contains the reference R/S line characterized with the Hurst exponent of 0.25. Position of relevant time moments: (1) - 3^h 38^m UT, (2) - 4^h 07^m, and (3) - 7^h 16^m are shown in the surveying frames. As one may see, variations in the noise structure (and hence, in its nature) were detected possibly caused by the nearby seismicity.

To conclude the report, we list the main results.

1. Natural EM signal of the ULF-ELF frequency range is an anti-persistent noise.

It's Hurst exponent equals 0.25 which proves that individual lightning strokes are independent.

2. Disturbances are present in the seismo-active region changing the structure of radio noise seen as abrupt variations of the R/S curves and of relevant Hurst exponent.

3. Additional studies are necessary to establish the nature of these disturbances.

References

1. Nickolaenko A.P., C. Price, and D.D. Iudin, Hurst exponent derived for natural terrestrial radio noise in Schumann resonance band, *GRL*, 27, 3185 - 3188, 2000.
2. Turcotte, D.L., *Fractals and Chaos in Geology and Geophysics*, Second edition, Cambridge University Press, Cambridge, UK, 1997.

K. HATTORI⁽¹⁾⁽²⁾, *Y. AKINAGA*⁽³⁾, *M. HAYAKAWA*⁽³⁾,
K. YUMOTO⁽⁴⁾, *T. NAGAO*⁽⁵⁾, *S. UYEDA*⁽²⁾

1. Marine Biosystems Research Center, Chiba University, c/o Department of Earth Science, Faculty of Science, Chiba University, Chiba 263-8522, Japan

2. International Frontier Program on Earthquake Research, Institute of Physical and Chemical Research (RIKEN),
c/o Earthquake Prediction Research Center, Tokai University, Shimizu 424-8610, Japan.

3. Department of Electronic Engineering, The University of Electro-Communications, Chofu 182-8585, Japan

4. Department of Earth and Planetary Science, Faculty of Science, Kyushu University, Fukuoka 812-8581, Japan

5. Earthquake Prediction Research Center, Tokai University, Shimizu 424-8610, Japan

ULF MAGNETIC ANOMALY PRECEDING 1997 KAGOSHIMA EARTHQUAKES

Abstract. Spectral analysis have been performed for ULF magnetic data associated with 1997 Kagoshima earthquakes observed at Tarumizu Station. The variations of magnetic field intensity and polarization at the period of local midnight time (00:00-04:00L.T.) have been investigated and suggested that there are obvious anomalies preceding two moderate earthquakes (M6.5 and M6.3) in comparison with those of remote reference stations of Chichijima and Darwin. The apparent increase of the vertical component S_Z has been observed a few weeks before the first earthquake on March 26, 1997. The increase is found to be about 1.0×10^{-3} nT/ $\sqrt{\text{Hz}}$ and this situation lasted one week before the second earthquake. The values of polarization found to increase about one month before the first earthquake. The earthquake occurred at the stage of decreasing of polarization values. These observational facts suggest that these activities around two Kagoshima earthquakes seem local phenomena, which corresponds to the earthquake related ULF magnetic anomalies.

1. Introduction

Electromagnetic phenomena associated with big earthquakes are recently considered as promising phenomena (e.g. Hayakawa and Fujinawa, 1994, Hayakawa, 1999). One of the most promising methods is a method of analyzing earthquake related ULF emissions because convincing evidences of ULF magnetic signature have been reported (e.g. Fraser-Smith et al., 1990, Kopytenko et al., 1993, Hayakawa et al., 1996). In this paper, we will present results of ULF emissions for big earthquakes occurred at Kagoshima region, Japan, 1997. Two moderate earthquakes occurred at 17h31m L.T. on March 26, 1997 (U.T. = L.T. - 9hours), and 14h38m (L.T.) on May 13, 1997, respectively. The Japan Meteorology Agency (JMA) reported that the magnitude of former

earthquake was 6.5 and latter one was 6.3 and their depth were less than 20 km. Their epicenters were located at the geographic coordinates (32.0N, 130.3E) and (31.9N, 130.3E), respectively. A fluxgate type magnetometer measuring 3 components of geomagnetic fields with 1 Hz sampling rate, was in operation at Tarumizu Station (31.48N, 130.72E), which belongs to Kyushu University. The distances between the observatory and epicenters are about 60 km. The geographical relationship between the ULF magnetic station and epicenters of earthquakes is shown in Fig. 1. The ULF instrument is composed of three ring core type fluxgate magnetometers (H (NS), D (EW), and Z (vertical) component) and the waveform data are recorded. The detailed information on the ULF magnetometer system is reported by Yumoto et al. (1992). In this paper we will report on ULF

magnetic phenomena associated with Kagoshima earthquakes.

2. Procedure of Data Analysis

We analyzed data from August 19, 1996 to September 13, 1997. The seismic activity is also shown in Fig.1. The active seismic zones are divided into 3 regions, which are Kagoshima region, Hyuga region, and Tanegashima region, respectively. The epicenter distance to Hyuga and Tanegashima regions are about 100km and the

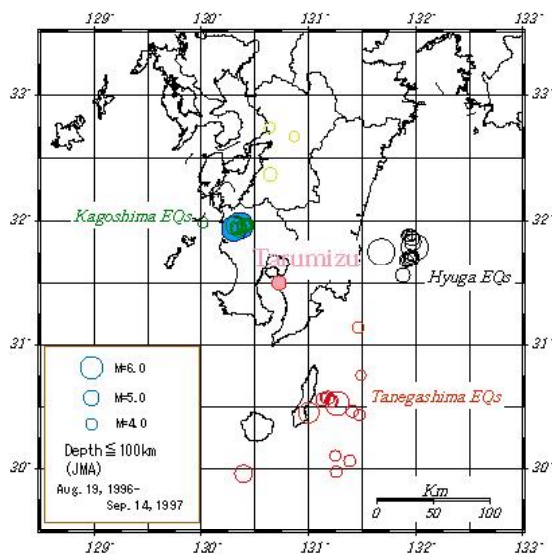


Fig. 1 The relation between Tatumizu station and epicenter.

strongest earthquakes in both Hyuga and Tanegashima region were M6-7. It is very important to extract subterranean effects from the geomagnetic field data in order to clarify the relationship between earthquakes and ULF magnetic activity. The observed data have been analyzed in a similar manner as reported in Hayakawa et al.(1996a). (1) The data observed in the midnight (L.T. = 00h - 04h) have been used because the artificial disturbance is considered to be much smaller than in daytime. (2) Spectral analysis based on FFT method with 30 minutes interval has been applied to waveforms of three magnetic field components. There are 8 units for one day. (3) The mean value and standard deviation σ for obtained frequency spectrum have been calculated over the whole analyzed period to estimate the superior

frequency range as earthquake related ULF emissions. (4) In order to distinguish subterranean effects from the phenomena of geomagnetic pulsation more clearly (Hayakawa et al., 1996a), a variation of a spectral density ratio of vertical and horizontal components such as S_Z/S_H have been investigated. We call this procedure polarization analysis. The average over 8 FFT units in a certain frequency band have been taken as a daily value. (5) The data observed at the place far from the epicenter region and at the geomagnetic conjugate point have been analyzed in the same way to discriminate between local and global phenomena. (6) In order to estimate the contribution of geomagnetic pulsations, the daily variation of ΣK_p , where K_p indicates global geomagnetic activity during every 3 hours and ΣK_p corresponds to the daily sum of K_p , have been investigated. When $\Sigma K_p > 30$, the geomagnetic activity is active.

3. Observational Results and Discussions

In order to investigate whether the obtained ULF magnetic phenomena is global or local activity, the data observed at Chichijima station, which locates at Chichijima Islands (27.15N, 142.30E), and at Darwin station, Australia which corresponds to the geomagnetic conjugate point (12.40S, 130.90E) have been analyzed as a remote reference data, simultaneously. Fig. 2 shows the location of stations. The same magnetometer system has been installed and operated at both station. The distance between the epicenter region of Kagoshima earthquakes and Chichijima station is about 1200km in the southeast direction. There is no big earthquakes with distance of 100 km from Chichijima and Darwin stations during the analyzed period. Figs.3 show the variation of spectral density of horizontal components S_G and S_Z , where S_G is the spectral intensity of a total horizontal component $((S_H^2+S_D^2)^{1/2})$ at frequency band of 0.01Hz. The variations of 10 days backward running mean of 0.01Hz band at Tatumizu, Chichijima, and Darwin stations are displayed with red, green, and purple

lines. Unfortunately, the remote reference data at Chichijima and Darwin stations were missing



Fig. 2 The relation of the epicentral region and remote reference stations.

around the period of two moderate Kagoshima earthquakes. The upper panel of Figs.3 indicates the variation of the horizontal intensity S_G and the lower one shows that of S_Z . The bottom one shows the variation of ΣKp index. It is found that the horizontal variations are quite similar for the stations of Tarumizu, Chichijima, and Darwin. On the other hand, the variation of the vertical component around the first earthquake is quite different among each other. At the conjugate point, the similar variation is expected for the global activities because the geomagnetic field line is same. The increase of the vertical component is about $1pT/\sqrt{Hz}$. Except this period, the variation between Tarumizu and Darwin looks like quite similar. We cannot say in detail because of data missing, however it seems

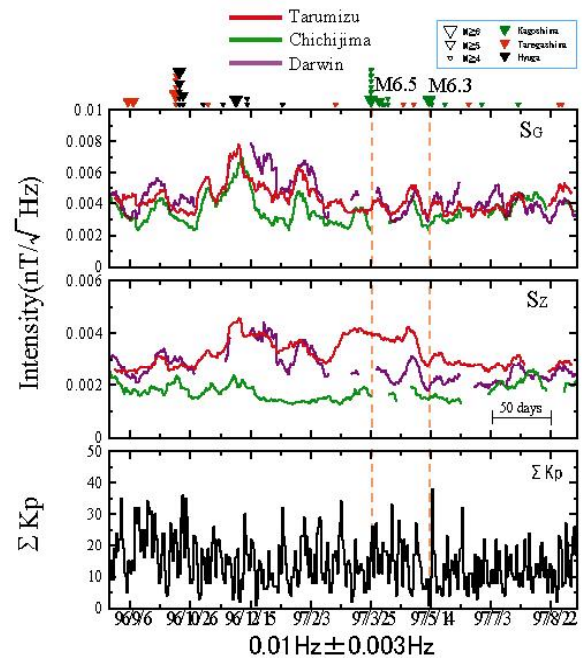


Fig.3 The variations of spectral intensity at 0.01Hz band. (a) S_G (b) S_Z , and (c) ΣKp . The variation of 10days backward running mean of daily values is plotted.

that the variation of Darwin station around March 10 and differences of the shape and the slope of onset in the end of February might be informative about this.

Figs. 4 show the daily variation of polarization in the same manner as Figs. 6. The upper panel indicates S_Z/S_G and the middle one shows the local seismicity, around Tarumizu station which reveal the daily sum of released energy within 90 km in terms of magnitude. The bottom one shows a variation of ΣKp index for the analyzed period. As for S_Z/S_G , the polarization values at Chichijima and Darwin stations are found to be very stable and distributed between 0.6 and 1.2. On the other hand, those at Tarumizu station are found to be increased up to 2 which is almost twice of ordinary level of 0.9 before the first earthquake. As for S_Z/S_G , the polarization values at Chichijima and Darwin stations are found to be very stable and distributed

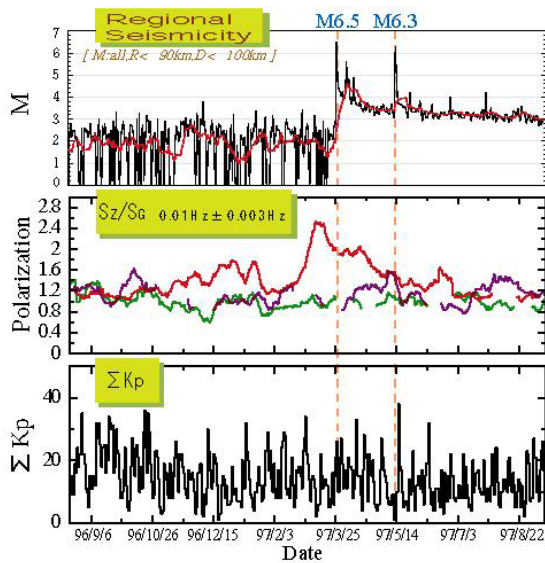


Fig.4 The variations of polarization at 0.01Hz band. (a) S_G/S_Z , (b) regional daily sum of seismicity in terms of magnitude and (c) ΣK_p . The variation of 10 days backward running mean of daily values is plotted for polarization. As for the seismicity, the black and the red lines show the daily variation of the regional seismicity and variation of 10 days backward running mean of the daily values.

between 0.6 and 1.4 and between 0.8 and 1.6, respectively. On the other hand, those at Tatumizu station are found to be increased up to 2.5 which is almost twice of ordinary level of 1.1. We can also notice that S_Z/S_G at Kagoshima station increases gradually from October, 1996 which corresponds to almost 5 months before the first earthquake and it calmed down once at the end of January, 1997. And

suddenly it jumped up in the end of February in comparison with remote stations. Then, it seems to be recovered at the beginning of July, 1997.

Therefore, the enhancement of S_Z and polarization at Kagoshima station is considered to be local phenomena. Furthermore, we can recognize the similar double peaks in local seismicity. Anomalous changes in polarization are seemed to be preceded the actual seismic activity. The leading time is found to be a few weeks. Moreover, there have been no significant magnetic disturbances one month before two moderate Kagoshima earthquakes in general. Therefore, obtained ULF magnetic anomalies seem to have no relationship with geomagnetic storms and these facts are highly suggestive of a possibility of connection with the seismic activity of Kagoshima region.

It is very important in order to eliminate global effects from observed ULF data in the point of monitoring of earth crust activity. The usage of data from multiple stations, especially the remote reference site and/or the magnetic conjugate site are very intrinsic. But the data observed at stations distributed near the epicenter are also informative on spatial correlation of ULF anomaly associated with earthquakes. Furthermore they might also provide us a key for penetration/propagation effects, which seem to be strongly connected with the underground structure, that is conductivity. Of course, it is very significant to remove artificial effects in Japan. These are future problem.

References

1. Fraser-Smith, A. C. et al., Geophys. Res. Lett., 17, No.9, 1465-1468, 1990.
2. Hayakawa, M. and Y. Fujinawa, Editors, "Electromagnetic Phenomena Related to Earthquake Prediction", Terra Scientific Pub. Comp., Tokyo, 1994.
3. Hayakawa, M., et al., Geophys. Res. Lett., 23, 241-244, 1996.
4. Hayakawa, M., Editor, "Atmospheric and Ionospheric Electromagnetic Phenomena Associated with Earthquakes", Terra Scientific Pub. Comp., Tokyo, 1999.
5. Kopytenko, Y. A., et al., Phys. Earth Planet. Inter., 77, 85-95, 1993.
6. Yumoto, K., et al., J. Geomag. Geoelectr., 44, 261-276, 1992.

НЕТРАДИЦИОННЫЕ ВИДЫ ЭЛЕКТРОМАГНИТНЫХ ИЗЛУЧЕНИЙ И ИХ ВЗАИМОСВЯЗЬ С ПРОБЛЕМОЙ ЭМС ТЕХНИЧЕСКИХ СРЕДСТВ

Abstract In the paper the structure of the electromagnetic external acting factors (EM EAF) are considered. The untraditional types of electromagnetic radiation are highlighted. The possibility of joining within the framework of one standard or group of the standards of experimental actions from traditional and untraditional sources of radiation are considered. It is illustrated on an example of new structure of the standards, designed TC 77 IEC on EMC the TS. The integrated system of the standards IEC on EMC TS will be able become key formation joining all possible types of EM EAF

С 80-х годов резко обострилась проблема защиты электромагнитных технических средств (ЭМ ТС) от снижения качества функционирования, вызываемого внешними воздействующими факторами электромагнитного происхождения (ЭМ ВВФ).

Это, во-первых, связано с изменениями в облике современных ЭМ ТС как на микроуровне (элементная база), так и на макроуровне (большие компьютерные сети, глобальные сети АСУ, объединенные электроэнергетические системы и т.п.), что обуславливает высокую их восприимчивость к воздействию ЭМ ВВФ.

Во-вторых, за этот период произошли большие изменения в структуре источников ЭМ ВВФ и их характеристиках. Современное представление источников ЭМ ВВФ дано в таблице.

В 1992 г. ТК-77 МЭК (электромагнитная совместимость электрооборудования, включая электрические сети) в международном стандарте МЭК 1000-4-92 (ГОСТ 29280-92 установил номенклатуру репрезентативных испытательных воздействий. В ее состав включены 23 вида помех, объединенных в 6 групп. Эти помехи квалифицированы как обобщенный результат воздействия традиционных источников электромагнитных полей и токов естественного и искусственного происхождения.

За последнее десятилетие наряду с известными источниками электромагнитных излучений (ЭМИ) появился ряд нетрадиционных типов излучателей (см. таблицу). Среди них можно выделить две подгруппы источников ЭМИ.

Первая подгруппа включает источники ЭМИ ядерного происхождения (ядерные источники ЭМИ). Электромагнитное излучение высотных ядерных взрывов распространяется на большие расстояния (до сотен км) и воздействует не только на военные, но и гражданские объекты. Поэтому их влияние на гражданские технические системы нельзя не учитывать.

В 1992 г. ПК-77С в составе ТК-77 МЭК (включая Россию) начал разработку комплекса международных стандартов по обеспечению защищенности гражданских объектов и систем от воздействия ЭМИ высотного ЯВ, который не является традиционным источником ЭМИ. Характеристики некоторых ядерных источников ЭМИ приведены в стандартах МЭК 61000-2-9, МЭК 61000-2-10 и МЭК 61000-2-11/1/. В стандартах МЭК 61000-4-23 и МЭК 61000-4-32,33 приведены соответственно методы и средства испытаний гражданских объектов на стойкость к воздействию ЭМИ ВЯВ /1/.

Вторая подгруппа источников нетрадиционного ЭМИ включает ставшие известными в 90-е годы различные модификации нелетального электромагнитного оружия и средств электромагнитного террора. К ним

относятся следующие виды мощного ЭМИ-излучения:

- источники на основе традиционных генераторов и фазированных антенных решеток, суммирующих мощности отдельных СВЧ генераторов в узконаправленный пучок СВЧ излучения;
- источники квазиизотропного, в т.ч. широкополосного СВЧ излучения на основе взрывомагнитных генераторов;
- СВЧ генераторы на релятивистских электронных пучках;
- мощные сверхширокополосные импульсные антенны (Ultra Wide Band Source).

За последние годы произошел качественный скачок в области создания мощных сверхширокополосных направленных излучателей электромагнитной энергии с шириной спектра 50 МГц÷10 ГГц /2,3/. Особенно активные

разработки в этой области ведутся в Philips Laboratory (USA) /4/.

С помощью направленного сверхширокополосного источника ЭМИ можно подавить технические средства управления и связи, а также осуществлять широкополосную локацию малозаметных целей, использующих для своей защиты технологию «Стелс».

Обеспечение защиты ЭМ ТС от ЭМ ВВФ не может быть эффективным без проведения их испытаний на устойчивость ко всему спектру воздействий, приведенных в таблице. Виды электромагнитных помех, которые могут создаваться в военных средствах технических систем и объектов гражданского назначения, не укладываются в номенклатуру испытательных воздействий, установленных МЭК 1000-4-92. В связи с этим возникает необходимость расширения указанной номенклатуры и дополнение ее видами испытательных воздействий от нетрадиционных источников ЭМИ.

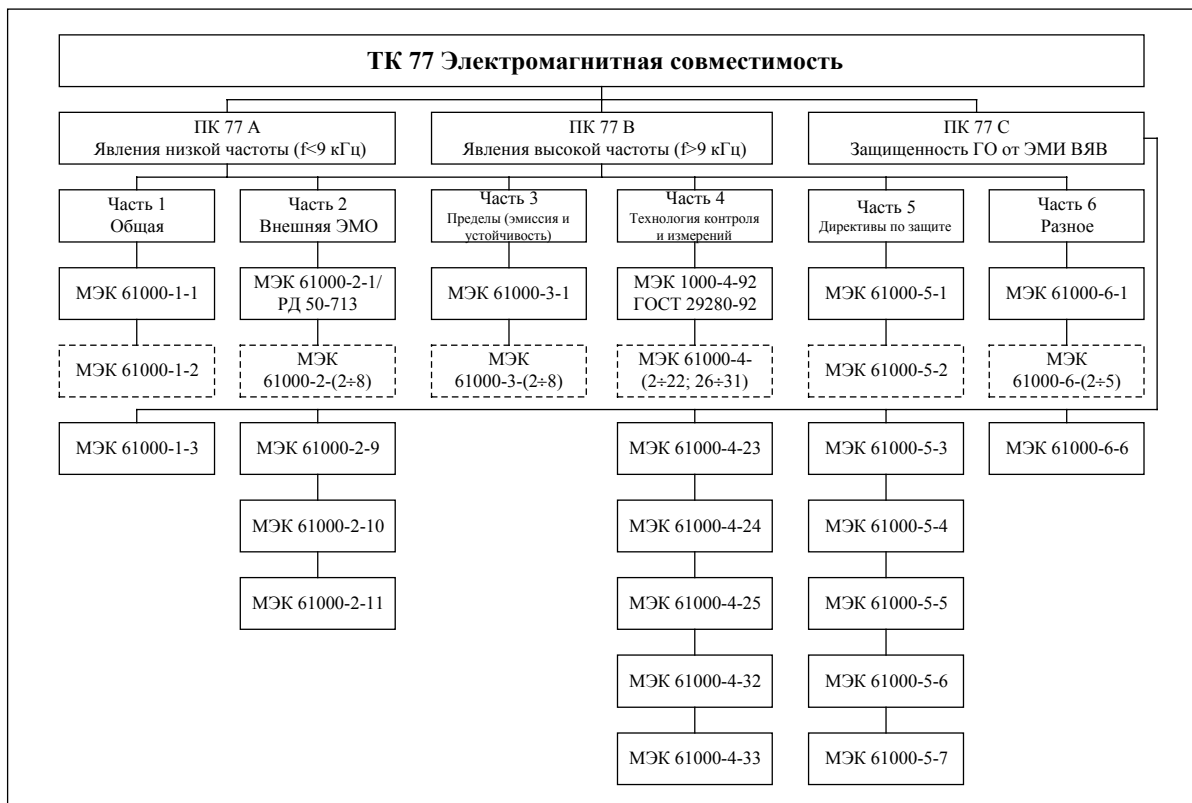


Рисунок. Интегрированная система стандартов МЭК по ЭМС ТС (концепция ТК 77)

С другой стороны, увеличение количества видов испытаний, очевидно, приводит к возрастанию экономических затрат на разработку помехоустойчивых ТС.

Возможными путями их снижения могут быть следующие/5/:

Таблица. Источники внешних воздействующих факторов электромагнитной природы (ЭМ ВВФ)

Подклассы						
Естественного происхождения			Искусственного происхождения			
Группы						
Земные процессы		Внеземные процессы	Нетрадиционные источники ЭМИ		Технические системы	
Подгруппы						
Разряды атмосферного электричества	Разряды статического электричества	Вспышки Солнечной Активности	Ядерные Источники ЭМИ	Неядерное источники ЭМИ	Индустриальные средства	Радиопередающие средства
Виды						
Прямой разряд молнии	Прямое воздействие ЭСР	Мировые Геомагнитные бури	ЭМИ НЯВ	Средства РЭБ	ЛЭП	Радиопередающие станции
Непрямой Разряд молнии	Непрямое воздействие ЭСР	Геомагнитные Суббури	ЭМИ АЯВ	Направленные ультракороткие широкополосные излучатели	Оборудование подстанций	Радиолокационные станции
Разряд молнии между облаками			ЭМИ ВЯВ	Генераторы СВЧ излучений	Коммутационные процессы	
			СБ-ЭМИ ВЯВ	Средства электромагнитного террора	Электрофизические установки	
			ВЭМИ ЯВ		Силовые потребители	
			ГСЭМИ ЯВ			

– систематизация близких по характеристикам видов испытательных воздействий и адаптация их под однородные виды помех;

– объединение в рамках одного стандарта или группы стандартов испытательных воздействий от традиционных и нетрадиционных источников излучений. Примером такого подхода может служить разработка новой версии стандартов Германии по ЭМС-VG-95379-95, в которой объединены требования по защите от ЭМИ ЯВ и ЭМС ТС.

Принципиально возможность такого расширения разрешена ГОСТ 29280-92, в котором в п.4.6 указано:

«Допускается применение видов испытаний из числа регламентированных международными, зарубежными национальными и отечественными нормативными документами, не приведенными в настоящем разделе, а также дополнительных испытаний, учитывающих со-

вместное воздействие нескольких видов помех на ТС».

Техническим комитетом МЭК ТК 77 разработана интегрированная система стандартов по ЭМС ТС (рисунок). Новая структура стандартов МЭК состоит из шести разделов, в которые органически включены стандарты по защищенности гражданских объектов от ЭМИ ВЯВ. По состоянию на январь 2001 года в структуру включены 15 стандартов, в том числе: в 1 раздел - один, во 2 раздел - три, в 4 раздел – пять, в 5 раздел - пять, в 6 раздел – один стандарт. Новая система может стать ключевым образованием, объединяющим все возможные виды ЭМ ВВФ. Свидетельством реализации такого подхода является, например, предложение в проекте стандарта МЭК 61000-4-25 использовать для испытаний ТС на устойчивость к некоторым видам помех от ЭМИ ВЯВ соответствующие репрезентативные испытательные воздействия, определенные стандартом МЭК 1000-4-2-92.

Литература

1. W.A. Radasky, MW Wik.IEC Standardization of immunity light power transient phenomena. Book of abstracts. EUROEM 2000. 30 may- 2 June 2000, Edinburg.
2. Book of abstracts. AMEREM'96, Albuquerque, New Mexico, USA, may 1996.
3. Book of abstracts. EUROEM'98, Tel Aviv, Israel. June 14-19, 1998.
4. DVGGiri ID. Smith, KE Baum etc “A Reflector Antenna for Radioing Impulse-Like Waveforms”/ 4 July, 1995, Pro-Tech, Pulse Sciences, Phillips Laboratory.
5. Остафийчук Р.М., Остафийчук Н.А., Куприенко В.М., Мельников В.А. “Основные направления и формы взаимной адаптации практики обеспечения защищенности гражданских объектов от МЭМП ЕИ, оборонных объектов от ЭМИ ЯВ и электромагнитной совместимости их технических средств”. Сборник докладов VI Российской НТК, ЭМС-2000, С-Пб, 2000.

G. G. CHAVKA, K. ANISEROWICZ

Technical University of Bialystok, Faculty of Electrical Engineering
Grunwaldzka 11/15, 15-893 Bialystok, Poland

ANALYSIS OF TIME-DOMAIN CHARACTERISTICS AND SPECTRAL PARAMETERS OF SELECTED MODELS OF LIGHTNING CURRENT

Abstract. The analysis of time-domain and spectral characteristics for double exponential and polynomial models of the lightning current acting on any object is presented in the paper. The results of computation and analysis of pulse parameters are shown. The properties of the computed spectrum of the lightning models are discussed. It is considered the influence of the pulse time parameters on different bands of the lightning spectrum. A process of simulation of lightning surge on given object using the Discrete Fourier Transform is discussed. The received results may be used for the analysis of different EMC tasks.

1. INTRODUCTION

The analysis of properties of lightning threat belongs to the most important EMC problems. For EMC tests of radio- and electro-nic equipment influenced by the lightning discharges it is necessary to investigate the time-domain properties and the frequency-domain characteristics of LEMP. The lightning electromagnetic field components in both time and frequency domains are known and defined in several international standards [1-4]. However, the peculiarities of spectral frequency parameters of a lightning current pulse have been insufficiently taken under consideration, that it is necessary for the numerical calculations of lightning current action on different constructions and equipment [5].

The full analysis in the frequency domain is very important in the computations and proceeding the inverse Fourier transform [6, 7]. It helps to make the proper choice of the width of the lightning current spectrum and the step of computations in the time domain. At least first resonance of the equipment constructions should be included during numerical analysis.

In the paper, the analysis of time domain characteristics and the spectral parameters of the different lightning current waveforms have been presented. Two lightning current wave-forms have been taken under consideration: a double exponential model and a “polynomial” model. Exact parameters of these models have been computed for different lightning discharges as sources of EMC disturbances.

2. MODELS OF LIGHTNING CURRENT

In this paper, two models of lightning discharge current are considered. The first model is the double exponential model (DEXP) of the lightning waveform (Fig.1):

$$i_L(t) = I_m k (e^{-\alpha t} - e^{-\beta t}), \quad (1)$$

where I_m – maximum value, α , β – parameters, k – correction factor:

$$k = 1/i(t_{\max}), \quad t_{\max} = \ln(\beta/\alpha)/(\beta - \alpha) \quad (2)$$

t_{\max} – maximum value time of pulse.

The second type is the “polynomial” model of the lightning current waveform (Fig.2):

$$i_L(t) = \frac{I_m}{\eta} \frac{(t/\tau_1)^{10}}{1+(t/\tau_1)^{10}} e^{-t/\tau_2}, \quad (2)$$

where τ_1 , τ_2 – parameters, η – correction factor.

The base time parameters of lightning current models as standard shows are [1 - 4]:

front time – $t_{fr} = 1.25(t_2 - t_1)$, where t_2 and t_1 are the 90% and 10% points on the leading edge of the waveform, respectively (Fig.1,2);

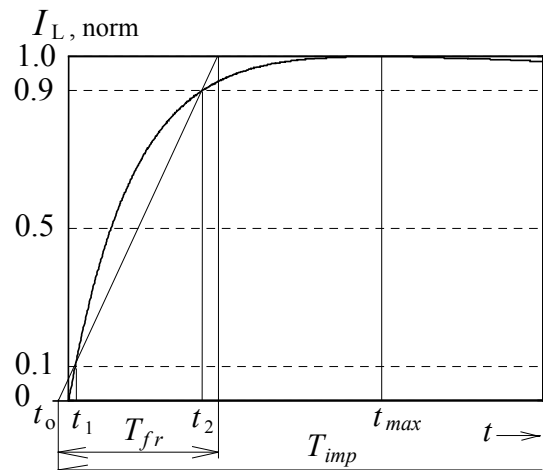


Fig. 1. Double exponential model

time to half value (half-decay time) – the time between the virtual zero time (t_0) and the time when the waveform reaches half of the peak value during the decay ($t_{0.5}$) (Fig.3):

$$T_{imp} = t_{0.5} - t_0, \quad t_0 = 0.125(9t_1 - t_2).$$

It is known [1-4] that the β factor in (1) and τ_2 in (2) determine basically the pulse front time, and the α factor and τ_1 in (2) – the half-decay time of the lightning current pulse; usually, $\alpha \ll \beta$, $\tau_1 \ll \tau_2$.

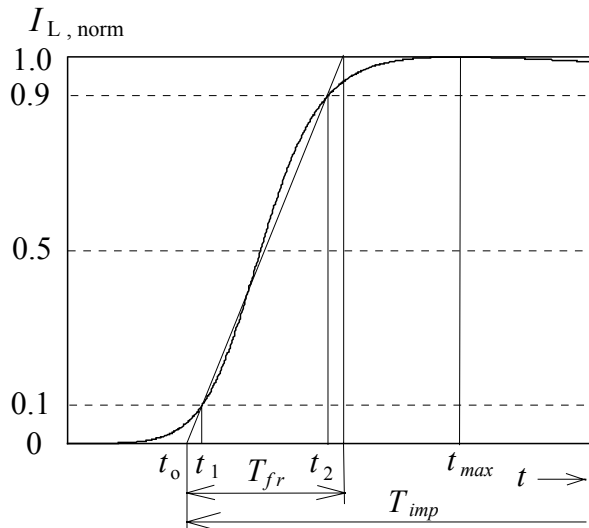


Fig. 2. Polynomial model of the lightning waveform of the lightning waveform

Table 1. Parameters for double exponential model

t fr, μs	t imp, μs	$\alpha \cdot 10^{-4}$, s ⁻¹	$\beta \cdot 10^{-6}$, s ⁻¹	k	t _{max} , μs
1.2	50	1.4732	2.0810	1.043	2.396
2.0	25	3.3687	1.0622	1.156	3.355
2.0	50	1.5292	1.1888	1.072	3.710
0.25	100	0.6986	10.840	1.005	0.678
1	200	0.3517	2.6727	1.010	2.485
10	350	0.2127	0.2461	1.051	19.48

Table 2. Parameters for polynomial model

t fr, μs	t imp, μs	τ_1 , μs	τ_2 , μs	η	t _{max} , μs
1.2	50	2.2716	68.528	0.9406	3.8153
2.0	25	4.0414	30.899	0.8080	5.9838
2.0	50	3.8670	66.507	0.9030	6.1687
0.25	100	0.4552	143.27	0.9928	0.9466
1	200	1.8320	284.85	0.9863	3.5730
10	350	19.046	475.66	0.9300	31.436

3. PARAMETERS OF THE LIGHTNING CURRENT MODELS

There are different lightning discharge waveforms in the real threats [1 - 4]:

- the first positive stroke 10/350μs;

- the subsequent negative stroke 0.25/100μs;
- the first negative stroke 1/200μs,
- other lightning surges 2/50μs, 2/25μs, 1.2/50.

The first parameter above is the front time, and the second - the half-decay time of the pulse.

In this work the exact values of time parameters are computed for the standard determinations (Fig.1,2) for the above pulses. These values are shown in Tables 1, 2.

As it is may be seen the obtained values are some differ from the published in literature [1-4]. Historical reasons (the calculation for 30% and 90% points) and a precision of previous calculations may explain this.

There are some differences between two models of the lightning pulses (Fig.1, 2).

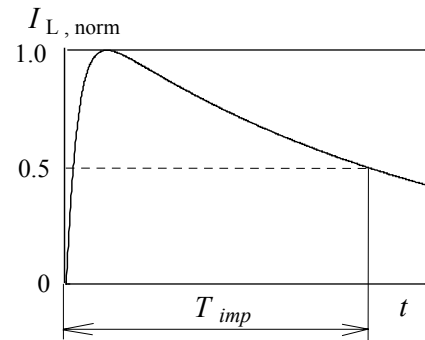


Fig. 3. Half-decay time of lightning pulse

The double exponential model is simpler than the polynomial one, but the derivative of the first model does not reach zero in an origin. In the turn, the derivative is zero in the origin of the polynomial model, but there is some shift of the pulse. Therefore there are different values for t_{max} for these models (Table1, 2).

A full analysis of α and β parameters for different conditions of the lightning discharges for DEXP model is presented in [5].

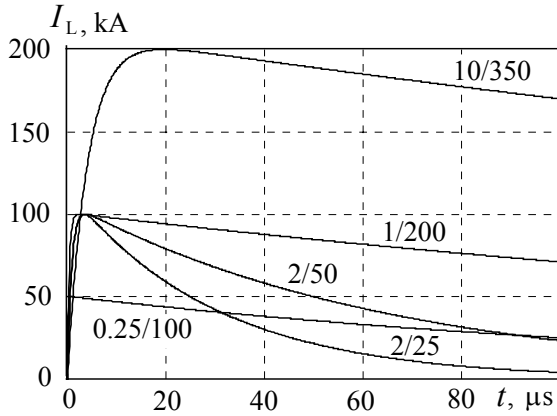


Fig.4. Double exponential model of lightning current pulse

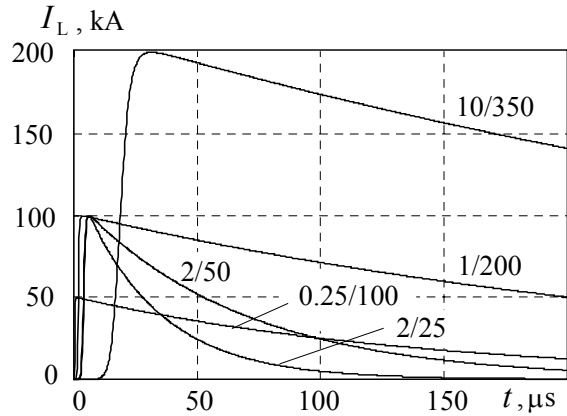


Fig.5. "Polynomial" model of lightning current pulse

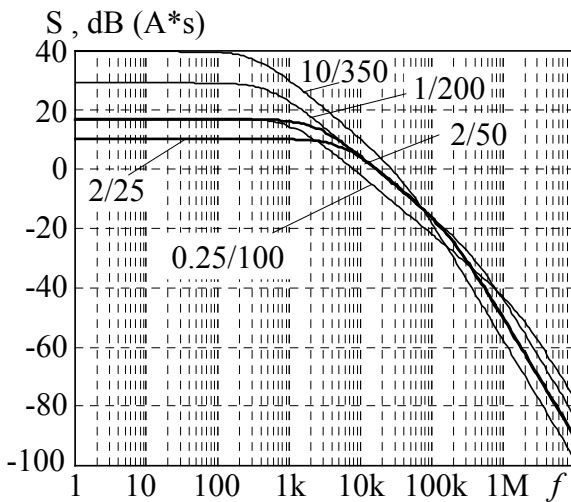


Fig.6. Amplitude spectrum of the lightning pulses

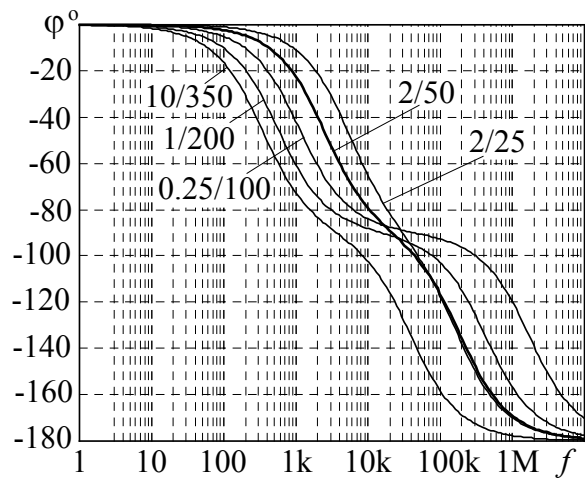


Fig.7. Phase spectrum of the lightning pulses

4. TIME- AND FREQUENCY-DOMAIN CHARACTERISTICS OF THE LIGHTNING CURRENT MODELS

The time-domain characteristics of the lightning discharges for both models are shown in Fig.4, 5. As it may be seen the pulses have almost common zero point for the double exponential model; but for the polynomial model the pulse shift depends on the half-decay time of the lightning current pulse.

The spectral amplitude and phase characteristics corresponding to assumed values of the pulse maximum (Table 3) are presented in Fig.6, 7. The zero of the amplitude spectrum is at level of 1A*s.

We see from these figures that the values of the front time and the half-decay time have the influence on *different parts* of the spectrum.

Table 3. Maximum values of the lightning pulses

I_m , kA	Pulse parameters
200	10/350
100	1/200
	2/50
	2/25
50	0.25/100

The *front time* values determine the shape of the spectrum in the band of *large frequencies* only up to 1...10 MHz for the levels lower than about (-20dB) for the given parameters of the pulses. This means that the spectrum width for large amplitude values does not almost depend on the front time value.

On the other hand, the *half-decay* time values define the spectrum shape at *small frequencies* only, smaller than ~10 kHz.

In this band the biggest amount of the whole energy of the lightning strike is concentrated. This means that the half-decay time influences the large components of the amplitude spectrum only.

The smaller the values of front time and half-decay time the greater the width of the corresponding part of the spectrum (Fig.6, 7).

This information is very important for the analysis of the lightning surges and for the lightning protection of different constructions, equipment, masts, including various radio-communication objects. In this case the Discrete Fourier Transform (DFT) is used for simulation of the time-domain characteristics of the given object during the lightning discharge.

Investigations of the lightning spectrum help us to formulate the criterion of reconstruction quality of the time-domain characteristics from the pulse spectrum samples. In particular, it concerns the choice of the step in the frequency domain and number of indispensable frequency components.

It can be shown that the front time value defines the whole frequency domain for the analysis of lightning pulse model and the given stroked object. On the other hand the half-decay time value determines the step of analysis in the frequency domain [5].

The *smaller the front time* values and *greater the half-decay* values of the lightning pulse the *greater* the necessary frequency band and *smaller* the frequency step for the analysis of the given object.

In addition, one must take into consideration the possible resonances, the influence of electromagnetic radiation and the mutual

coupling between different parts of the analyzed stroked construction or the object in accepted frequency band [6,7]. Thus the time and applied computer power restricts the possible range of simulation of these tasks, including the analysis of overvoltages appearing in the constructions and the equipment.

The considered lightning pulses, their analytical models and the results of time- and frequency-domain computations may be used for tests of given objects in any laboratory, too.

5. CONCLUSION

In the paper, there is presented the analysis of time-domain characteristics and spectral parameters based on the double exponential and the polynomial models of the lightning current waveforms acting on the given object. The time parameters of the lightning current models have been calculated and compared to these known from the literature. Some inaccuracies have been shown.

The properties of the spectrum of the lightning models have been discussed. It is considered the influence of pulse time parameters on different parts of the lightning spectrum. A process of synthesis of the current waveform and the simulation of lightning surge on given object using the Discrete Fourier Transform (DFT) is discussed.

The received results and elaborated recommendations for the time and spectral parameters may be used for the prediction of lightning threat to any objects and for analysis of the other different EMC tasks.

References

1. IEC 61312-1, International standard, "Protection against lightning electromagnetic impulse", 1995.
2. VG 96 901 "Nuclear electromagnetic pulse (NEMP) - and lightning protection", 1985.
3. R.B.Standler, "Protection of Electronic Circuits from Overvoltages", J. Wiley & Sons, N.Y., 1989.
4. В.И.Кравченко, "Грозозащита радиоэлектронных средств", Радио и Связь, 1991.
5. G.Czawka, K.Aniserowicz, M.Zielenkiewicz, "Analysis of time and frequency parameters of lightning current pulse acting on radiocommunication systems", Proc. of XIV State Symposium of Telecommunication, KST-98, v. D, p. 317-323, Bydgoszcz, 1998.
6. G.Chavka, K.Aniserowicz, Computer simulation of action of lightning current on the construction of antenna masts, 14th Intern. Symposium on EMC-98, str.481-485, Wroclaw, 1998.
7. G.Chavka, K.Aniserowicz, Secondary electromagnetic field during lightning discharge to radiocommunication object, Proc. of IV Intern. Symposium on EMC-2001, St.Petersburg, Russia, 2001.

ACKNOWLEDGEMENT

The authors would like to acknowledge the support of this work by the State Committee for Science Research of Poland under the Rector's Projects W/WE/1/98 and W/WE/5/00.

G. G. CHAVKA, K. ANISEROWICZ

Technical University of Bialystok, Faculty of Electrical Engineering
Grunwaldzka 11/15, 15-893 Bialystok, Poland

SECONDARY ELECTROMAGNETIC FIELD DURING LIGHTNING DISCHARGE TO RADIOCOMMUNICATION OBJECT

Abstract. The results of computation of the secondary electromagnetic field distribution in the near zone of the radiocommunication antenna mast during a lightning stroke has been presented. The mathematical model of the object under investigation has been shortly described. The antenna model of the lightning channel has been implemented. The results of example computation of currents and radiated fields in the selected zones have been discussed. The received results may be used for the analysis of the EMC threat to the radiocommunication object.

1. INTRODUCTION

The analysis of the radiocommunication object under the conditions of the lightning action is one of the very important EMC problems. The prediction of lightning current flow in metal segments of the antenna support construction and the analysis of near electromagnetic field distribution may show the most threatened zones of the object. Hazards due to conducted or induced overvoltages may be estimated when surge fields and currents are known. The computations similar to the presented below are helpful while designing the overvoltage protection of the electronic equipment.

There are many publications concerning the lightning current distribution in the conductors of the lightning protection systems (LPS). The contributions may be classified into two main groups according to the applied mathematical models of LPS. The authors use either the simplified lumped-circuit models (including only the inductance of wires) or the complicated field-theory models. Still, the analyses of the lightning threat of the radiocommunication sites, concerning both current and electromagnetic field surges, need to be developed.

In the presented work some computations were made using the field-theory approach. The presented model makes it possible to predict the currents and fields, taking into ac-

count the resonant properties of the analysed structure.

2. NUMERICAL EXAMPLE

Consider the radiocommunication site shown in Fig. 1. Assume that the ground is ideal (high conductive). The antenna mast is 150 m high and it has three levels of guys equally spaced as it is drawn in Fig. 1.

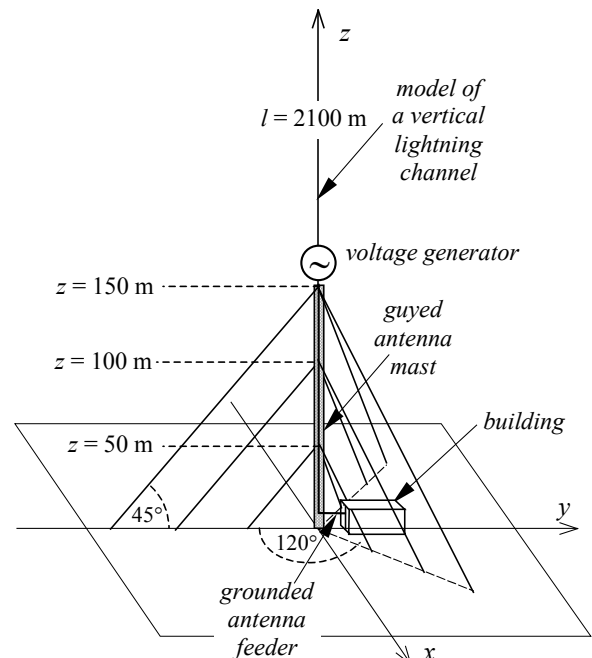


Fig. 1. Example to be analysed

The diameter of guy ropes is 40 mm. The dimensions of the building lightning protection system are shown in Fig. 2. The LPS wires diameter is 8 mm.

The point of the lightning stroke was chosen to be at the top of the mast.

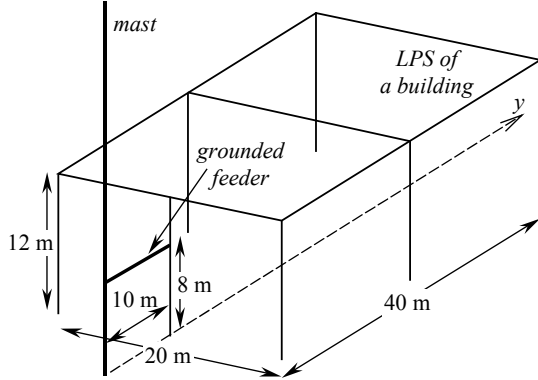


Fig. 2. Dimensions of the LPS of the building

An antenna model of a lightning channel has been applied [6]. This model consists of the long vertical wire with the ideal sine voltage source at the bottom. Such a way of inserting of the generator makes it possible to model the upward movement of the return stroke current. Only voltage sources may be modelled using the method implemented in the used computer code. The enforced current was achieved by successive computations in the frequency domain basing on the mixed-potential equations combined with the method of moments for the polynomial approximation of the currents.

Mathematical model, combining the incident field \mathbf{E}^i with the current distribution and with the scattered field \mathbf{E}^s , \mathbf{H}^s , comes from the equations formulated in frequency domain:

$$\mathbf{E}^s = -j\omega \mathbf{A} - \nabla\Phi \quad (2)$$

$$\mathbf{H}^s = \frac{1}{\mu_0} \nabla \times \mathbf{A} \quad (3)$$

$$\mathbf{A} = \mu_0 \iint_S \mathbf{J}_S \frac{e^{-jkR}}{4\pi R} dS \quad (4)$$

$$\Phi = \frac{1}{\epsilon_0} \iint_S \rho_S \frac{e^{-jkR}}{4\pi R} dS \quad (5)$$

$$\nabla \cdot \mathbf{J}_S = -j\omega \rho_S \quad (6)$$

The voltage generator (Fig. 1) has been introduced using the boundary condition on the conductor surface:

$$\mathbf{n} \times \mathbf{E}^s = -\mathbf{n} \times \mathbf{E}^i \quad (7)$$

The influence of radiation of the wires and the mutual coupling between the segments has been considered automatically during the integral equations formulation.

The computations have been run as follows. First compute the current transmittance, defined as a quotient of the current spectrum in the analysed point divided by the current spectrum at the bottom of the lightning channel model, for the drive of frequency independent 1V generator. This transmittance equals to the current in the given point for the enforced 1A frequency independent current source. Then the current spectrum in the given point has been achieved as a product of the computed transmittance and the spectrum of the lightning current pulse.

The Discrete Fourier Transform has been used to obtain the current waveforms in the time domain. 512 spectrum samples with the interval of 5 kHz in the frequency domain were taken into account. Thus the analysed frequency band reaches 2.56 MHz, that allows to include several resonances of the explored structure during computations.

The double-exponential equation has been introduced to describe the lightning waveform:

$$i(t) = k I_0 (e^{-\alpha t} - e^{-\beta t}) \quad (8)$$

The lightning waveform has been chosen to be 100 kA, 2/25 μ s that has been achieved by substituting: $k = 1.166$, $\alpha = 3.4 \times 10^4$ 1/s, $\beta = 1.0 \times 10^6$ 1/s. These parameters fit in the range of the real lightning parameters. Due to the choice of the 100 kA peak value it is easy to calculate the percentage distribution of currents and fields. The 2/25 μ s waveform lets us to make a clear show of the resonant properties at the graphic output.

3. RESULTS OF COMPUTATIONS

The results of computations both in the frequency and time domains are presented below. The field distribution may be shown for any frequency chosen from the considered spectrum. The sample plots of the electric and magnetic field spectrum for $f = 320$ kHz, $z = 1$ m above ground are shown in Figures 3–6.

The plots of the radiated fields in the time domain “captured” for $t = 3 \mu\text{s}$ are presented in Fig. 7 – 10. The field waveforms along the $\pm y$ axis are shown in Fig. 11 – 14.

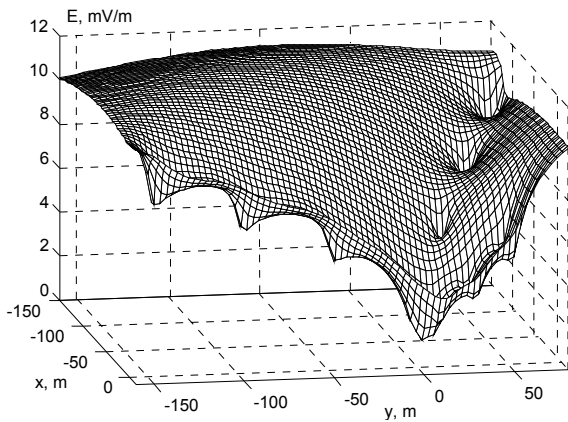


Fig. 3. $E(f=320\text{kHz})$, 1m above ground

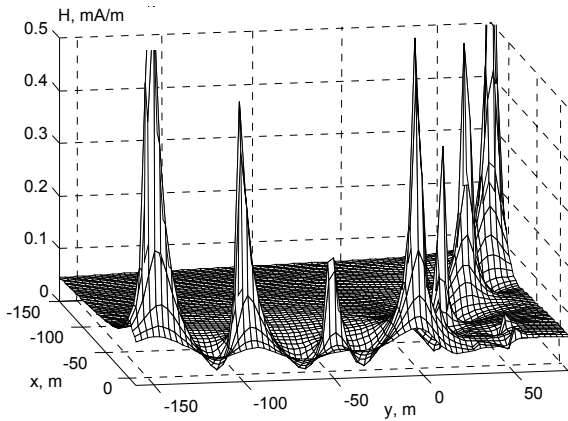


Fig. 4. $H(f=320\text{kHz})$, 1m above ground

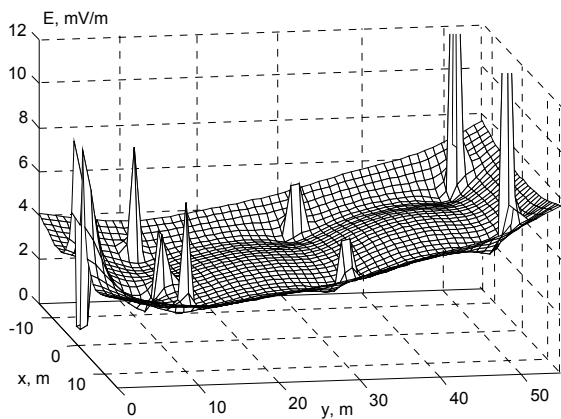


Fig. 5. $E(f=320\text{kHz})$ near the building ($z=1\text{m}$)

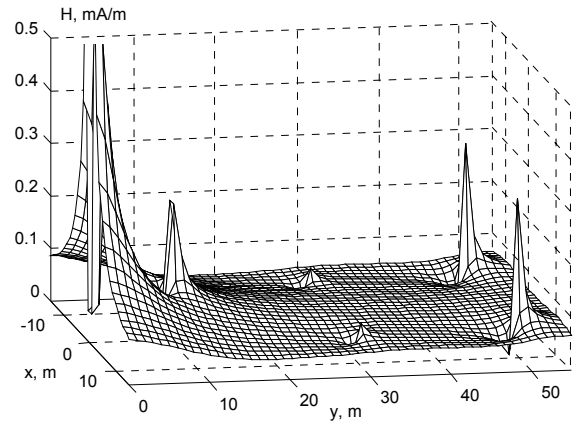


Fig. 6. $H(f=320\text{kHz})$ near the building ($z=1\text{m}$)

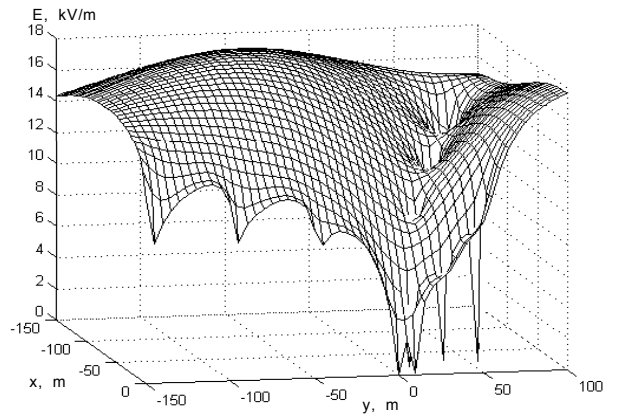


Fig. 7. $E(t=3\mu\text{s})$, 1m above ground

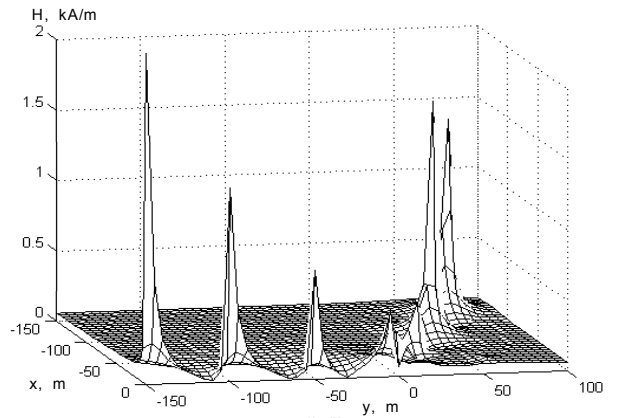


Fig. 8. $H(t=3\mu\text{s})$, 1m above ground

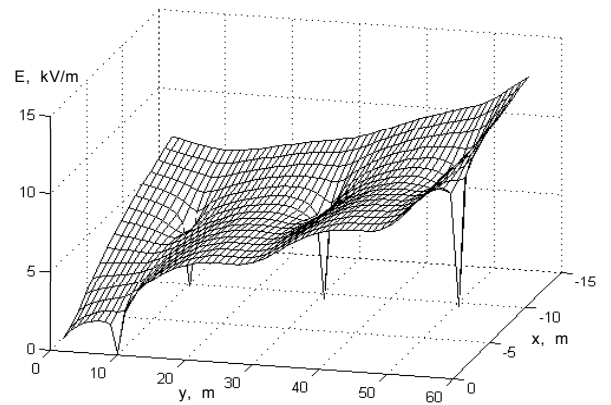


Fig. 9. $E(t=3\mu\text{s})$ near the building ($z=5\text{m}$)

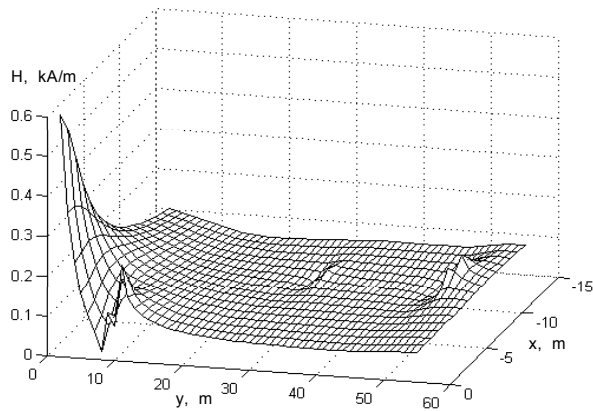


Fig. 10. $H(t=3\mu\text{s})$ near the building ($z=5\text{m}$)

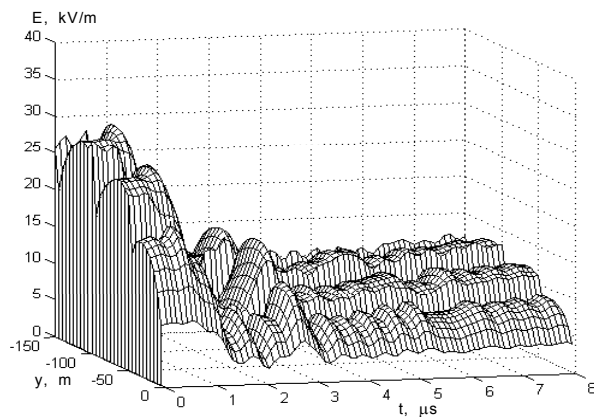


Fig. 11. E-field along $-y$ axis, 1m above ground

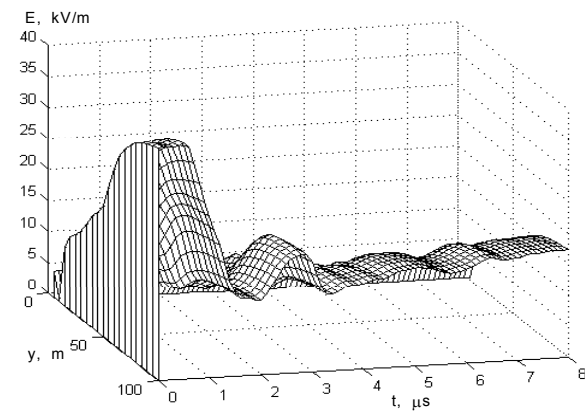


Fig. 12. E-field along $+y$ axis, 1m above ground

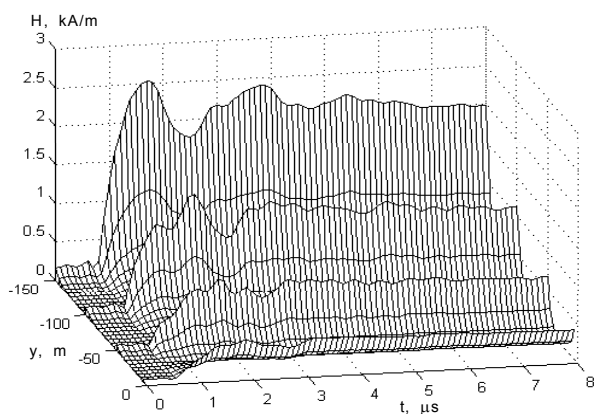


Fig. 13. H-field along $-y$ axis, 1m above ground

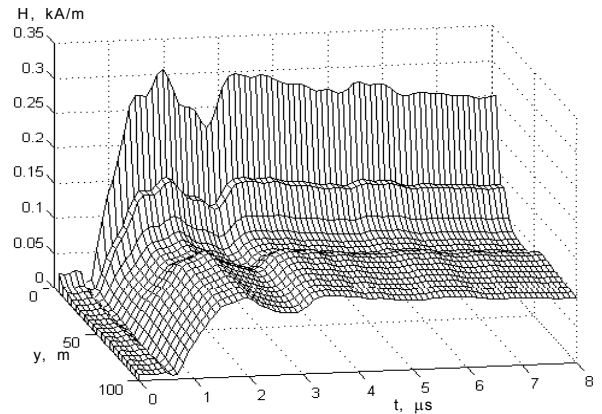


Fig. 14. H-field along $+y$ axis, 1m above ground

The plot of the current waveform changes in the time domain down the tower of the mast is presented in Fig. 15.

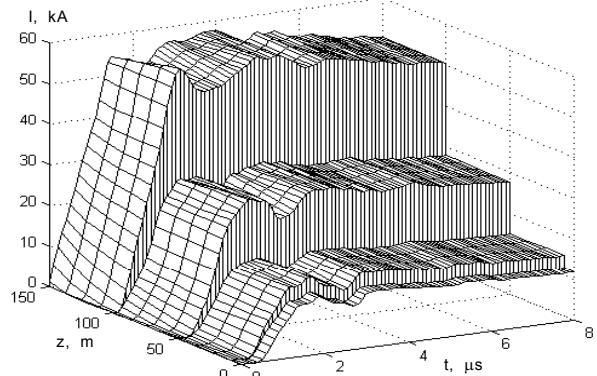


Fig. 15. Current waveform changes along z axis

4. CONCLUSION

The presented method makes it possible to compute the lightning currents in metal segments of the object and the distribution of the near electromagnetic fields.

The resonant properties of the structure have been distinctly shown in the presented figures.

The maximum computed values reach some tens of kilovolts per meter for the E-field and some kiloamperes per meter for the H-field.

The guy ropes cause significant reduction of the lightning threat near the bottom of the mast.

The received results may be used for the prediction of the lightning threat to the radio-communication objects.

References

1. G. G. Chavka, K. Aniserowicz, "Computer simulation of action of lightning current on the construction of antenna masts", 14th International Wroclaw Symposium and Exhibition on EMC, June 23-25, 1998, pp.481-485.
2. A. R. Djordjević, M. B. Baždar, T. K. Sarkar, R. F. Harrington, "Analysis of Wire Antennas and Scatterers (AWAS)", Artech House, London, 1995.
3. IEC-61312-1, International standard, "Protection against lightning electromagnetic impulse", Part 1: "General principles".

ACKNOWLEDGEMENT

The authors would like to acknowledge the support of this work by the State Committee for Science Research of Poland under the Rector's Projects W/WE/1/98 and W/WE/5/00.

K. ANISEROWICZ¹, M. ZIELENKIEWICZ²

¹ Technical University of Bialystok, Faculty of Electrical Engineering
Grunwaldzka 11/15, 15-893 Bialystok, Poland

² Center of Protection Against Overvoltages and Electromagnetic Interferences
Grunwaldzka 11/15, 15-893 Bialystok, Poland

OVERVOLTAGE PROTECTION OF STATIONARY RADIOCOMMUNICATION OBJECTS

Abstract. The review of principles of overvoltage and lightning protection of stationary radio-communication objects has been reviewed. New methods of protection against overvoltage/lightning threats to these objects have been discussed. Important aspects of the overvoltage protection have been pointed out. The paper has been written in compliance with the series of international standards, e.g. IEC 61024, IEC 61312.

1. INTRODUCTION

The overvoltage hazard of a typical site equipped with a tower or mast is significant. One of the very important problems is to ensure the personnel and equipment safety in the radiocommunication objects during the lightning/overvoltage action.

The greatest threat to radiocommunication objects is lightning. Therefore the proper lightning protection is also efficient against overvoltages caused by other sources, e.g. by industry breakdowns imposed to the AC lines.

There are several aspects that should be considered during planning the lightning and overvoltage protection. The most important aspects are: estimation of the possible electromagnetic threats, design of the lightning protection air terminations, grounding, equipotentialization, bonding, shielding, surge protective devices in coordination with the AC power supply system, overvoltage protection of RF cables and signal lines.

2. THE THREAT

There are published many research works and standards concerning the evaluation of overvoltage threats. In the IEC standards and other publications [1 – 5] the parameters describing levels of hazard have been specified. When talking about the radiocommunication facilities safety and reliability one should consider how to ensure the survival during hazards of the highest levels. The highest currents specified in [1 – 3] are as follows:

200 kA, 10/350 μ s – the first positive lightning stroke;

50 kA, 0.25/100 μ s – the subsequent negative strokes;

100 kA, 1/200 μ s – the first negative lightning stroke.

The other typical surge waveforms are:

– for currents – several kiloamperes, 8/20 μ s;

– for voltages – several kilovolts, 1.2/50 μ s.

The electromagnetic field may also cause damages and disturbances. The electric field strength close to the lightning channel reaches hundreds of kV/m and the magnetic field – several kA/m. In a distance of some hundreds of meters they are still measured in kilovolts per meter or hundreds of amperes per meter, respectively. The lightning electromagnetic pulse may cause damages in electronic circuits in a distance exceeding 1.5 km from the discharge channel.

3. PROTECTION OUTDOORS

One of the evident systems belonging to the means of outdoor protection is the building air termination system. There are many misunderstandings among engineers that concern the determination of the range of lightning protection zones. It is reasonable to plan the air terminations of the object's buildings with respect to the most restrictive requirements. Such requirements are given in [1] where the rolling ball concept is recommended (Fig. 1). The rolling ball radius is recommended to be between 20 m and 60 m that correspond to the protection efficiency levels between 98% and 80%, respectively. Though the smallest radius in proximity to high antenna supporting constructions (towers, masts) may be questionable, it has to be noted that the height exceeding 60 m is asserted to add nothing to the lightning protection zone at the ground level.

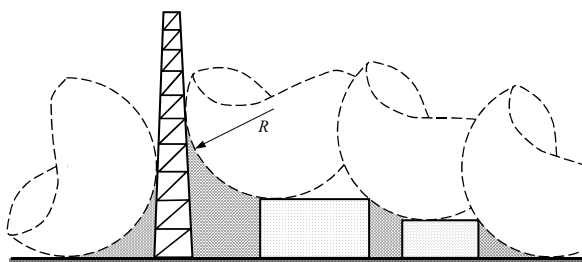


Fig. 1. The rolling ball concept

There exists the undoubted hazard for antennas to be hit. Some methods that allow increasing the lightning protection zone near the tower top are shown in Fig. 2. The additional air terminations should not distort the antenna characteristics.

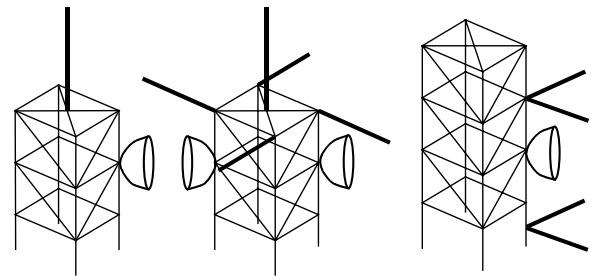


Fig. 2. Lightning protection of antennas

The conductors diverting the lightning current from the air terminations to the ground should be robustly connected to the earthing system. The quality of connections is of great importance for the effectiveness of protection. Avoid direct contacts between dissimilar metals (e.g. copper-steel, copper-aluminum) because of corrosion. The best quality of underground connections is achieved by exothermic welding.

The typical system of grounding electrodes is extensive (Fig. 3 – 4). The earthing system with the central point emphasis is the best solution. Typically the central point is located below the antenna tower or below the feeder entry to the building. The feeder entry needs to be equipped with the grounded bulkhead panel that is shortly described further (Fig. 5).

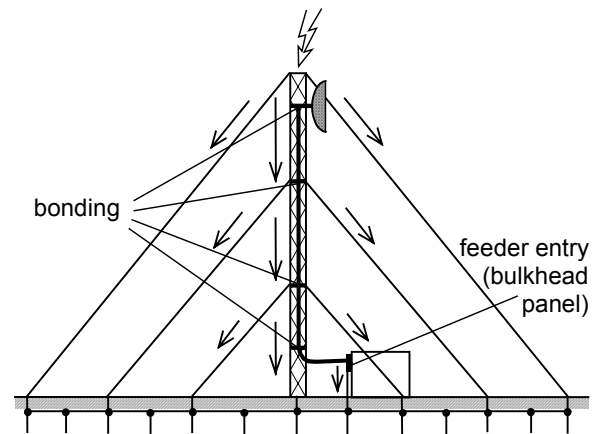


Fig. 3. Extensive central point grounding and feeder equipotential bonding to the mast

Radial horizontal grounding bars must run along the directions of the guy anchors and they must be well connected to the anchors and to the central point of the grounding system.

The properly designed grounding electrodes form the integral system connecting all the buried metal elements, including

grounded fence (Fig. 4). Such earthing mesh reduces the step voltage and prevents the danger of spark-over discharges in the soil during lightning stroke.

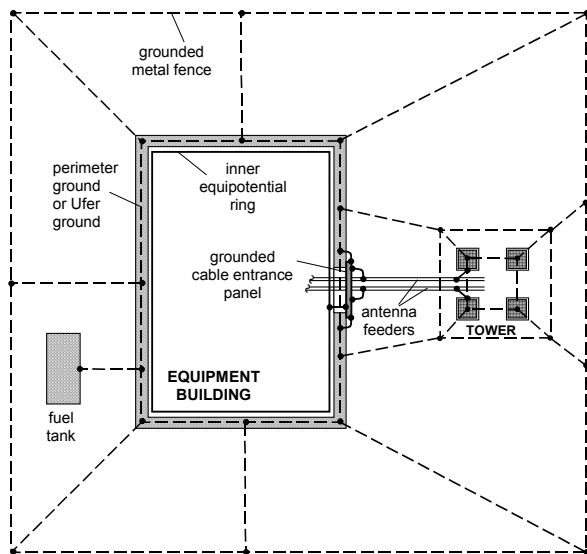


Fig. 4. Small site grounding

It is reasonable to supplement the horizontal grounding elements by vertical rods (Fig. 3). In many recommendations it may be found that such vertical elements cause the improvement of the dynamic properties of the grounding system. Moreover, the seasonal changes of the soil resistivity have lower influence on the grounding parameters if the system is equipped with the vertical rods. Popular vertical rods are made of steel electrolytic covered by copper. They are much more corrosion-resistant than the rods made of galvanized steel.

Many spark-over feeder damages have been reported because of great potential differences appearing between the tower and the feeders during lightning stroke. So the outdoor equipotentialization is the important means of protection. This is realized by bonding of the waveguides and RF feeder shields to the tower at least at each guy level (Fig. 3) to reduce the arriving voltages and to provide the controlled paths for the surge current. Such bonding at intermediate levels is recommended also for not guyed towers exceeding 60 meters high.

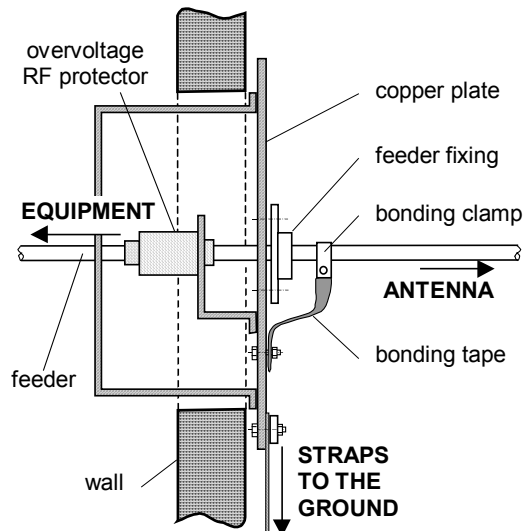


Fig. 5. Bulkhead panel (side view)

The best protection of RF equipment is achieved if the feeders enter the building below the ground level. Unfortunately, such solution is rarely possible. A good path to the ground for the lightning current flowing down the feeder shields is assured by installing the copper bulkhead panel at the entry to the apparatus building. The idea of the bulkhead panel is shown in Fig. 5.

Using copper straps is recommended to make bonds and paths to the ground. Straps have significantly less inductance than the comparably conductors with circular cross section. So, the surge voltage drop along the straps is lower that is seen from the formula:

$$u = L \frac{di}{dt} \quad (1)$$

4. PROTECTION INDOOR

One of the means of protection that can never be called to be overestimated is the equipotentialization inside the equipment building. Equipotentialization at the ground level concerns all the conductive installations of the site, including water pipes, sewerage and central heating system.

The best way to reduce the potential differences that arrive during lightning stroke is to install grounded copper bars or rings around the rooms containing the apparatus. Such equalizing rings are sometimes called the "halo grounds". All the transmitter/receiver chassis should be connected to

these rings using the shortest possible copper tapes or wires.

Sometimes in big radiocommunication sites the RF equipment may produce interferences of high level. One of the methods to reduce this problem is to make a grounded equipotential grid below the floor. This grid forms a kind of local “ideal ground”. All the apparatus chassis have to be connected to the grid.

The care for the bonding quality is strongly required. Direct contacts between dissimilar metals are not allowed. The known fact is that corrosion or bad quality may cause that such connections act as “diodes” producing many intermodulation problems in electromagnetic fields generated by the RF equipment.

The properly designed AC power supply system is of much importance in the fight against all the electromagnetic interferences. The AC network must be equipped with the overvoltage arresters. The example scheme of application of the two-step protection devices in the TN-C-S network is shown in Fig. 6.

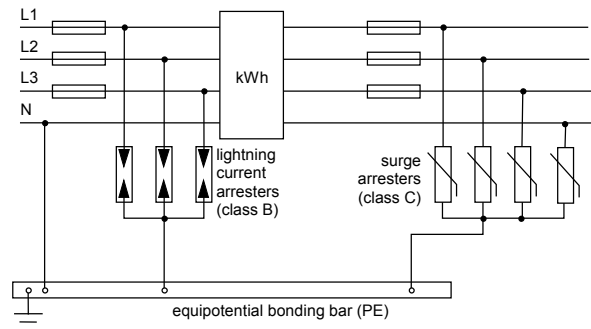


Fig. 6. Basic AC overvoltage protection (TN-C-S)

All the signal lines should be equipped with the overvoltage protection elements. This recommendation concerns telephone lines, monitoring, alarms, etc. The building inside should be divided into overvoltage protection zones. Locate the surge protection devices in the AC power system and in signal lines on the borders of protection zones.

The bulkhead panel is a border between the outdoor and indoor equipment. This is the best place to locate the overvoltage protectors in the RF coaxial cables. These are: the gas tubes, quarter-wave stubs, and high-pass filters.

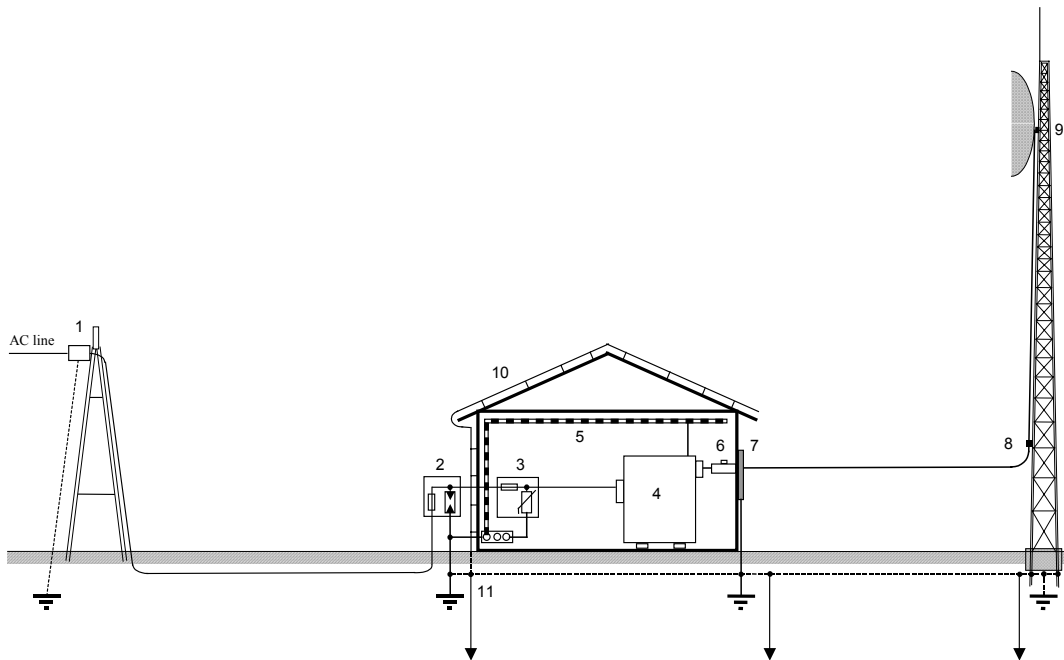


Fig. 7. Location of the basic overvoltage protection devices in the radiocommunication object with overhead AC power supply: 1 – AC overhead line surge arresters (class A), 2, 3 – AC overvoltage protectors (class B and C), 4 – T/R equipment, 5 – equipotential bonding bar, 6 – RF overvoltage protectors, 7 – bulkhead panel, 8, 9 – equipotential bonding, 10 – lightning protection system, 11 – grounding system

5. CONCLUSION

The basic concepts of lightning/overvoltage protection of radiocommunication sites have been pointed out. It is important to implement the new ideas into existing objects and while planning the new ones.

The summary of the main recommendations has been shown in Fig. 7.

The overvoltage protection is efficient if all the protective elements form a complete, logically designed system.

References

1. IEC-61024, Series of international standards, "Protection of structures against lightning".
2. IEC-61312, Series of international standards, "Protection against lightning electromagnetic impulse", Part 1: "General principles".
3. KTA 2206, "Auslegung von Kernkraftwerken gegen Blitzeinwirkungen", German standard.
4. MIL-HDBK-419A, "Grounding, Bonding and Shielding for Electronic Equipments and Facilities", 29 Dec. 1987.
5. "The "Grounds" for Lightning and EMP Protection", published by PolyPhaser Corp.

L. K. AUGUSTYNIAK

Białystok Technical University – Faculty of Electrical Engineering

LIGHTNING OVERVOLTAGES IN WIRING SYSTEMS OF THE BUILDING

During direct lightning strike into a building there is the injection of high impulsive currents in the lightning protection system (LPS) of the building. These high currents flow through down conductors resulting in a corresponding electromagnetic field, which can induce currents and voltages in loops of conductive installation inside the building. The induced voltages can be very high and may disturb or damage the electronic equipment. This paper presents the selected results of investigations of the induced overvoltages in low voltage power supply installation (LVPI) and structural cabling systems due to electromagnetic fields from surge currents in the LPS. The trials of numerical calculations of the induced overvoltages are also included.

1. Introduction

Lightning discharge is a major natural source of electromagnetic impulses, which interfere with the reliable operation of modern electronics and communication systems in both civilian and military applications. Lightning can interact with buildings basically in two ways: direct strikes and nearby strikes. Especially dangerous are overvoltages caused by direct lightning stroke to building.

Determination of the level of the threat for sensitive systems such as intelligent buildings, control and communication centres, modern hospitals, local area networks and other data transmission installations is an essential question.

Nowadays the most popular kind of wiring applied to complex systems of connections between electronic devices is structural

cabling. This is system of wiring, which makes possible realization of definite configuration of connections, but with possibility its future extensions and reconfiguration. Therefore wiring of a building without earlier knowledge of devices, which will be making use of wiring is possible. However every type of wiring of the building can create threat to devices connected to it as a result of induced overvoltages.

2. The problem of transients evaluation

During a direct lightning stroke to a building the surges in data-transmission and LVPI networks are induced by the electromagnetic field caused by lightning current propagating in the LPS or conducting elements of the building's construction. The level of interferences in a network strongly depends on the physical structure of the network itself. One of the biggest problems re-

garding the control of lightning induced overvoltages in data-transmission and low voltage power installations is the evaluation of the response of a complex wiring system to lightning electromagnetic pulses (LEMP).

There are many ways to evaluate the overvoltages caused by a direct lightning strike in a building, and many of them are theoretic studies, developed using analytical and numerical methods. Generally, the susceptibility of specific wiring system to transient waveforms of lightning origin is rather difficult and complex to calculate. Taking this fact into account, the investigations were made to estimate the levels and shapes of the induced overvoltages in low voltage power supply installation and structural cabling systems due to electromagnetic fields from surge currents in LPS.

3. Surge current injection

Selected results of the experimental studies on the LVPI and structural cabling network of UTP (category 5) cable are presented in this paper. The measurements were carried out on the real networks of a brick building. During research the current generator was connected to the bottom end of the perpendicular aluminium pipe about 7.7 metre long placed inside the building. The upper end of the pipe was connected to the air terminal of LPS on the roof of the object (node x on Fig. 1).

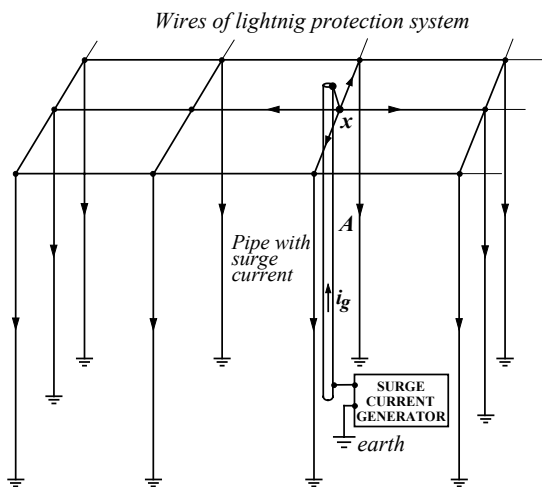


Fig. 1. Schematic diagram of experimental set-up for surge current injection

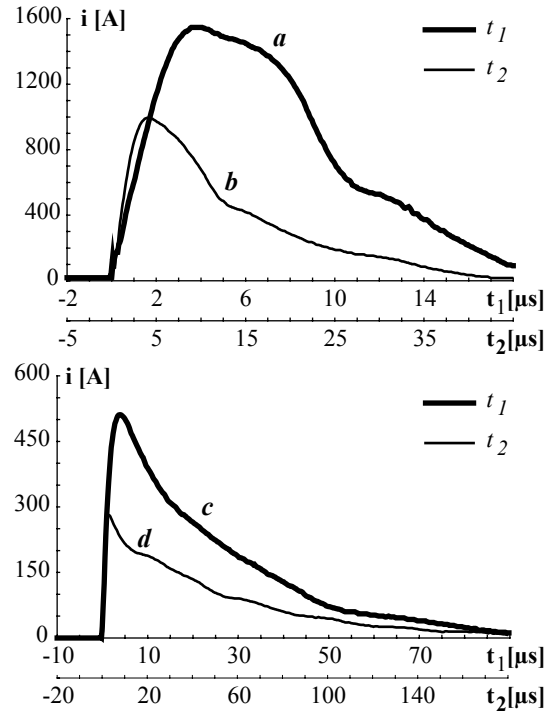


Fig. 2. Examples of measured injection surge current waveforms, which flew in the pipe and next in LPS

The second pole of the generator was jointed to earthing installation in the building. In this arrangement the surge current flowed into the aluminium pipe and subsequently in the building's LPS (Fig. 1).

In the research the peak values of surge currents in the pipe reached the values from several hundreds A to several kA. Some examples of surge current waveforms, which flew in the pipe, are presented in Fig. 2.

4. Overvoltage measurements

Overvoltage measurements were made in the circuits of real structural installation and LVPI arranged inside 2-storey building of brick. This permitted to avoid some errors (which would appear in model researches as a result of different simplifications) giving overvoltage image in typical installation.

The transverse and longitudinal induced voltages appearing in the structural and power supply installations were registered in selected sockets. Fig. 3 illustrates the measuring procedure in the structural installation. In the experimental study the wiring systems were completely disconnected from equipment. Measurements were taken in two

cases: without load and with load of 50 or 100 Ω .

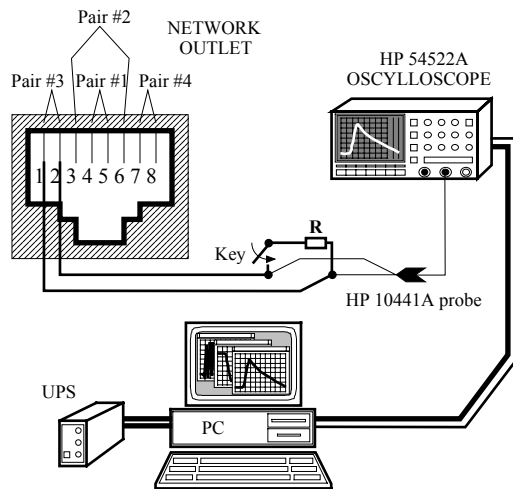


Fig. 3. The experimental set-up for the induced voltages measurement in the structural installation

Investigations showed high level of overvoltages induced in wiring by the simulated lightning current injected in the LPS of the building. At current peak value only 1.55 kA and rise time 2.5 μs voltages recorded in different points of installations had peak to peak values of some tens - some hundreds V.

Figure 4 presents example oscillograms of voltage waveforms registered in one socket of structural installation at test current peak value 1.55 kA and its rise time 2.5 μs (as in the graph *a* in Fig. 2.).

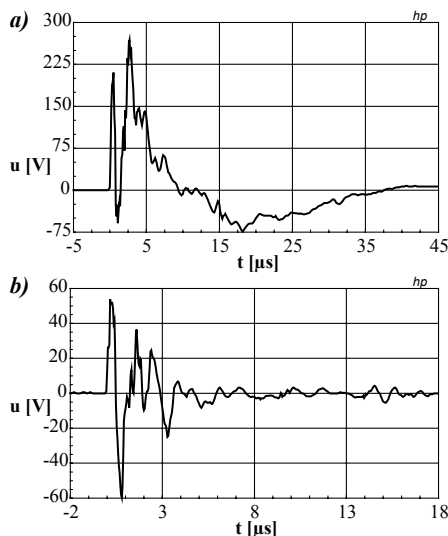


Fig. 4. Induced voltages recorded in one of structural installation sockets: a) without load, b) with load of 100 ohm

Figure 5 shows the example oscillograms of voltage waveforms registered in one socket of low voltage power installation at test current peak value 274 A and its rise time 1.2 μs (as in the graph *d* in Fig. 2.).

On the base of all registered in structural installation overvoltages some rules can be formulated:

- induced overvoltage values decreased with the length of line; the greatest values were registered in short sections of lines ending in rooms adjoining to the cross room; this may also result from the fact that the pipe with the full current was located 5 metres away from this cross room;
- if the line on a certain piece ran vertically (in parallel to the pipe with the surge current), overvoltage levels increased 2÷3 times;
- peak to peak values of overvoltages induced in structural wiring (with load $R = 100$ ohm) were on average about 1.5÷4 times smaller than in open circuit;
- overvoltage level in wiring grew about 2 times slower than value of test current.

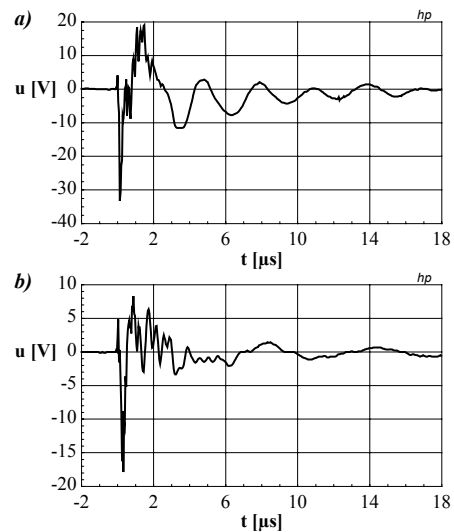


Fig. 5. Induced voltages recorded in one of LVPI sockets: a) without load, b) with load of 50 Ω

Registered overvoltage values grew with increasing the test current rise time. In spite of generating of current surges of different shapes and overvoltages registration in many points of installation it did not succeed to fix of distinct relation between the current rise time and the induced overvoltage level. The

installation itself may be the cause of these – its different parts ran different ways and in different horizontal directions and also in vertical direction in relation to the source of disturbances, therefore the resultant surge voltage being sum of voltages in different running sections of the line was accidental (similarly like in any other real installation).

5. Computer simulation

For comparison selected experimental events were calculated with AWAS (Analysis of Wire Antennas and Scatterers) com-

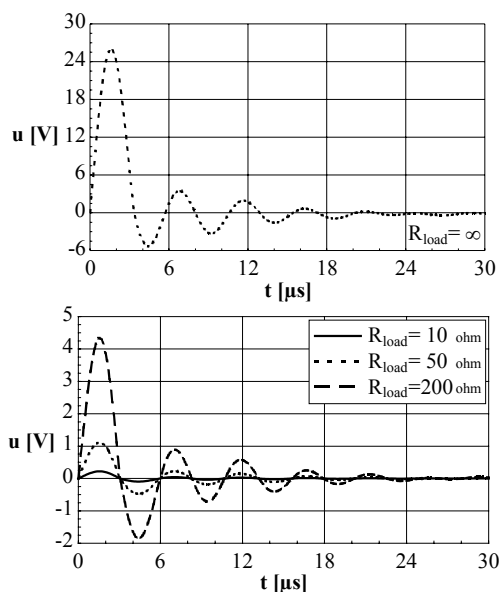


Fig. 6. Induced voltages in the same LVPI socket as in fig. 5 obtained from numerical calculation

puter program. The results of experimental investigations correspond with the results of numerical calculations obtained from a computer simulation of the real circuits and pulses. The examples of numerically calcu-

lated overvoltages in the same low voltage power installation socket as in Fig. 5 are presented in Fig. 6. The case concerns the injected current corresponding the graph *d* in Fig. 2 (the current peak value 274 A and its rise time 1.2 μ s).

6. Conclusions

Already in line segments from several to tens metres long, interconnecting devices inside the building, induced overvoltages of relatively high values can occur. Researches revealed high level of lightning overvoltages induced in LVPI and structural wiring by simulated lightning current flowing in LPS of the building. As earlier mentioned, note that at current peak value only 1.55 kA and rise time 2.5 μ s, the voltages registered in different points of installation had peak to peak values of some tens - some hundreds volts.

Attention should be paid, that in case of direct lightning strikes to buildings the real lightning currents have multiply higher peak values and shorter or similar rise times. Then the levels of overvoltages induced in wiring arranged inside the building will exceed considerably the electric strength of the equipment connected to wire installations and damage it. Some overvoltage measurements in real structural and power supply wiring, during lightning current distribution in LPS of the building, confirm possibilities of damages.

Only well-chosen overvoltage protection devices in LVPI and structural cabling systems assure the protection against this kind of danger.

References

1. Augustyniak L. K.: "Analysis of lightning overvoltages in computer networks inside buildings." Doctor's thesis, Technical University of Białystok, Białystok 1999.
2. Augustyniak L. K.: "Przebiegi atmosferyczne w instalacji oprzewodowania strukturalnego pojawiające się w skutek przeników z instalacji elektrycznej i rozplywu prądu piorunowego w instalacji piorunochronnej obiektu." V Ogólnopolskie Sympozjum Inżynieria Wysokich Napięć, Poznań-Kiekrz 2000, pp. 19÷24.
3. Harrison S., Wisdich M., Karmazyn H.: "Misapplication and poor installation of transient overvoltage protection." 23-rd ICLP, Firenze-Italy, September 23÷27 1996, vol. 2, pp. 628÷629.
4. Martzloff F. D., Tetreault M.: "Characterization of disturbing transient waveforms on computer data communication lines." 6-th Conference on EMC, Zürich 1985, pp. 423÷428.

ИЗМЕНЕНИЯ МИРОВОЙ ГРОЗОВОЙ АКТИВНОСТИ, НАЙДЕННЫЕ ПО ДАННЫМ ШУМАНОВСКОГО РЕЗОНАНСА

Непрерывные измерения шумановского резонанса выполнялись на станции Лехта в течение года (с августа 1999 по июль 2000г.). По накопленным данным построены средние динамические спектры поля, проведен анализ вариаций спектров и определены параметры мировой грозовой активности. Получены интегральные оценки суточных изменений уровня глобальных гроз и данные о сезонных изменениях активности в мировых грозовых центрах.

В настоящей работе представлены и обсуждены результаты годового электромагнитного мониторинга в диапазоне частот шумановского резонанса (ШР). Экспериментальные данные получены для трех компонент электромагнитного поля: вертикальной электрической (E_r) и двух ортогональных горизонтальных магнитных компонент (H_x и H_y). Компонента поля H_x ориентирована с запада на восток, а компонента H_y – вдоль направления север-юг. Напомним (см [1]), что в области частот ШР распространяются E -волны, у которых на поверхности земли отличными от нуля остаются компоненты E_r и H_φ . Спектр ШР состоит из ряда максимумов, расположенных на частотах около 8, 14, 20, 26 Гц. Ниже будет рассмотрены записи только магнитной компоненты поля.

1. Описание аппаратуры и пункта наблюдения. Непрерывные измерения проводились на станции Лехта (34 в.д., 64 с.ш.) Санкт-Петербургского филиала ИЗМИРАН в течение целого года: [август 1999-июль 2000г.]. Местоположение этой станции относительно трех известных мировых грозовых центров (МГЦ) таково, что азимуты азиатского, африканского и южноамериканского центров приблизительно равны 90^0 , 180^0 и 270^0 , соответственно. Такое географическое положение пункта наблюдения, а также то, что пики грозовой активности всех МГЦ приходятся на разное время суток (в 10 часов мирового времени - Азия, в 15 часов – Африка и в 20 часов - Америка) позволяет разделить информацию о грозовой активности по магнитной компоненте поля.

Так, максимальный вклад в амплитуду компоненты H_y вносят источники, расположенные на западе и востоке, т.е. в азиатском и американском МГЦ, а максимум чувствительности H_x приходится на южное и северное направления – следовательно эта компонента главным образом отражает активность в африканском МГЦ.

Блок-схема приемного комплекса описана в [2]. Магнитными антеннами служили индукционные датчики с ферромагнитным сердечником и встроенными антенными усилителями. Антенны ориентированы в направлении юг-север и запад-восток относительно географической системы координат. Электрическая антенна представляет собой изолированную металлическую сферу диаметром 40 см и емкостью ≈ 22 пФ, установленную на мачте высотой 3 м. Сигналы от датчиков передавались на вход приемника. Трехканальный приемник состоит из режекторных фильтров для подавления гармоник сети, масштабирующих усилителей, фильтров нижних частот.

Сигналы трех компонент поля после усиления и фильтрации подавались на вход многоканального аналого-цифрового преобразователя, установленного в компьютере и работающего под управлением программы, с помощью которой проводилась предварительная обработка, отображение средних и динамических спектров, временных форм принимаемых сигналов, а также накопление данных. Система работала круглосуточно в реальном масштабе времени.

Первичные данные представляют собой синхронные 12-секундные временные

формы сигналов трех компонент поля, оцифрованные с частотой дискретизации ≈ 170 Гц. После вычисления преобразования Фурье рассчитывались и усреднялись в течении каждых 10 минут энергетические спектры трех компонент поля $|E_r|^2$, $|H_x|^2$ и $|H_y|^2$. Полученная информация сохранялась на жестком диске.

2. Обработка спектров поля. В течение суток система сбора данных накапливала файлы с 10-минутными записями вышеуказанных величин. Исключения составляли промежутки времени, когда из-за ряда причин происходил сбой приемной аппаратуры. Из полученных 10-минутных записей некоторая часть была отбракована при последующей обработке.

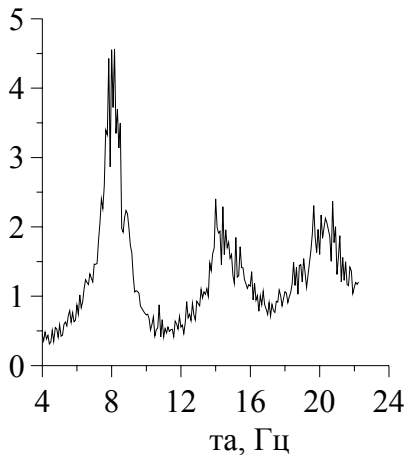


Рис.1. Типичный экспериментальный спектр $\langle |H_x(f)|^2 \rangle$

На рис.1 приведен типичный энергетический спектр ШР, полученный для компоненты H_x после отбраковки данных. При обработке отбраковке подвергались записи, искаженные помехами следующих двух типов:

- 1) Записи, спектры поля в которых имеют нерезонансную структуру, искаженные вследствие локальных широкополосных помех (близкие разряды молний, импульсные помехи, возникающие в силовой сети, вибрационные помехи и т.п.)
- 2) Записи, спектры которых искажены мощными узкополосными помехами в окрестности 25 Гц.

Отбраковка каждой из компонент поля для H_x и H_y проводилась отдельно и осуществлялась следующим образом. Выбирался день, для которого среди 10-минутных записей не встречалось помех первого или второго типа. Спектры $\langle |H_x(f)|^2 \rangle$ и $\langle |H_y(f)|^2 \rangle$, (за сутки накапливалось 144 спектра для каждой компоненты поля) были усреднены за эти выбранные сутки. Эти средние спектры принимались за эталон, а их типичная форма показана на рис. 2.

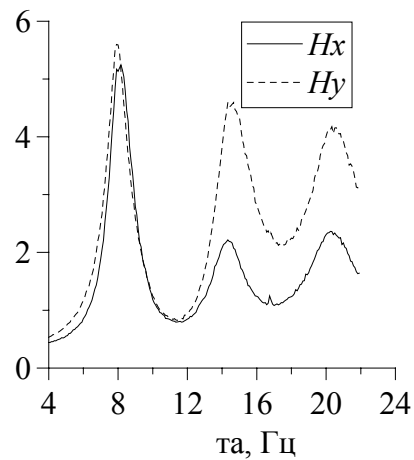


Рис.2. Эталонные спектры для $\langle |H_x(f)|^2 \rangle$ и $\langle |H_y(f)|^2 \rangle$.

Как видно из рисунка, усредненные кривые достаточно гладкие и имеют три хорошо выраженных максимума. Дальнейшая обработка заключалась в следующем. Каждый из накопленных 10-минутных спектров сравнивался с соответствующим эталоном. Если экспериментальная кривая выходила за границы коридора, верхняя и нижняя границы которого определялись как $F(f)/L$ и $F(f)*T$ соответственно, то она отбрасывалась как искаженная помехой. Здесь $F(f)$ обозначает эталонный спектр выбранной компоненты поля, $L=T=3.7$ – константы, значения которых были выбраны путем предварительного подбора. Если в каждой точке частотного диапазона [4 - 22] Гц значение экспериментальной кривой попадало в указанный коридор, то такой

спектр принимался в обработку. При этом дополнительно проверялось, не изменялся ли в момент записи коэффициент усиления (КУ) приемно-анализирующего комплекса, переключавшийся дискретно на 6 дБ. Если такое случайное переключение обнаруживалось, то оно компенсировалось программным путем, а запись шла в дальнейшую обработку. В течение года было обнаружено несколько незарегистрированных переключений КУ.

В результате такой отбраковки около 60 % данных были отброшены. К сожалению, из-за неполадок приемного канала, ответственного за H_y , июньская и июльская информация по этой компоненте была полностью испорчена. В марте 2000 г. оказалась испорченной информация для обеих компонент поля.

3. Результаты наблюдений. Для каждого месяца наблюдений были построены средние за месяц суточные профили энергетических спектров.

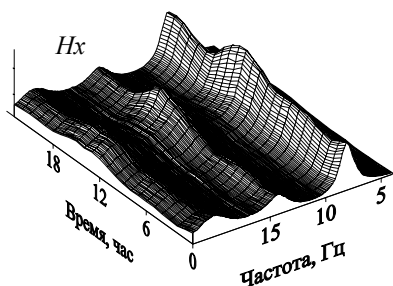


Рис.3. Средний за август суточный профиль $\langle |H_x(f)|^2 \rangle$

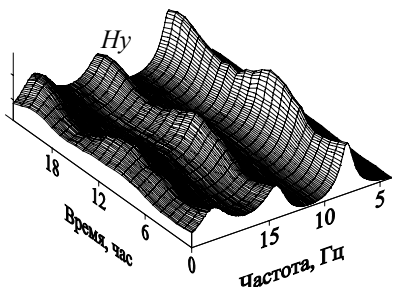


Рис.4. Средний за август суточный профиль $\langle |H_y(f)|^2 \rangle$

На рис.3 и рис.4 представлены профили энергетических спектров H_x и H_y для августа 1999 года. На графиках вдоль одной из горизонтальных осей отложено время суток по Гринвичу, вдоль другой горизонтальной оси отложена частота, измеряемая в герцах. Рисунки демонстрируют три шумановских резонансных мода, которые изменяются в течение суток как целое. Видно, что энергетические спектры на всех трех модах шумановского резонанса во времени ведут себя одинаково. Такие изменения свидетельствуют о том, что расстояние от наблюдателя до источников поля в течение суток существенно не изменяется (иначе изменялось бы соотношение амплитуд отдельных резонансных пиков), а все вариации амплитуда поля обусловлены изменениями уровня мировой грозовой активности.

Кроме того, в суточных вариациях компоненты H_x виден один максимум, отвечающий африканскому мировому грозовому центру. Изменения компоненты H_y содержат два максимума, один из которых (утро) обусловлен активностью азиатских гроз, а второй (вечер) – американскими источниками.

Вышесказанное верно для средних динамических спектров всех месяцев наблюдения, но структура спектров изменяется от месяца к месяцу. Такие изменения связаны с сезонным дрейфом мировой грозовой активности в меридиональном направлении.

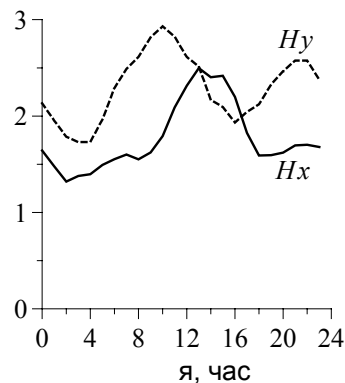


Рис.5. Средние за август суточные зависимости $\langle |H_x(T)|^2 \rangle$ и $\langle |H_y(T)|^2 \rangle$.

Поскольку интенсивность ШР спектров изменяется как целое, ее интеграл по частотам оказывается пропорциональным текущему уровню мировой грозовой активности. На рис.5 приведены интегралы энергетических спектров обеих магнитных компонент, полученные для августа 1999 года. Время суток по Гринвичу отложено по горизонтальной оси графика. Уровень мировой грозовой активности отложен вдоль ординаты в относительных единицах.

Как видно из рис.5, мировая грозовая активность представлена тремя грозовыми центрами. Интенсивность поля в компоненте H_x пропорциональна активности африканских гроз. Поле H_y пропорционально активности в азиатском и американском центрах. Максимум активности в Африке приходится примерно на 15 часов мирового времени, а в Азии и Америке – на 10 и 20 часов соответственно.

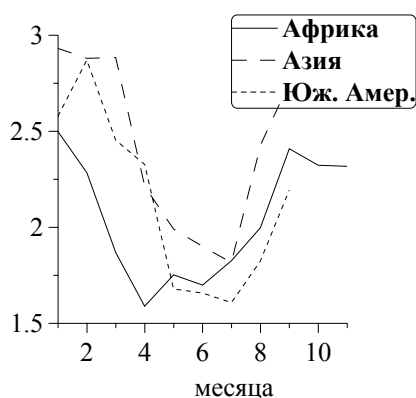


Рис.6. Динамика мировой грозовой активности.

Динамика мировой грозовой активности отражена также на рис.6. Здесь вдоль горизонтальной оси отложен порядковый номер месяца (1-август...12-июль), а вдоль вертикальной оси для всех трех МГЦ отложены максимальные значения интенсивности (в отн. ед.) Как видно, результаты наблюдений ШР_показывают, что далеко не всегда грозы в Африке являются наиболее интенсивными. Интенсивность мировых центров изменялась в

течение года в пределах от 1,8155 отн. ед. до 2,9305 для Азии, от 1,5879 до 2,4981 для Африки и от 1,6071 до 2,87 для Америки. Положения максимумов наблюдались в 9 ± 2 , 15 ± 2 и 20 ± 3 часов мирового времени соответственно. Необходимо отметить, что подобного рода оценки уровня мировых гроз можно получать только при СНЧ мониторинге и что такого рода измерения ведутся в настоящее время только в трех пунктах наблюдения, включая наши наблюдения в обсерватории Лехта.

4. Заключение. В заключение перечислим основные результаты работы.

1. Проведена обработка накопленного массива электромагнитных данных по шумановскому резонансу.

2. Выполнена отбраковка искаженных помехами данных и для каждого месяца в течение года непрерывных наблюдений получены средние динамические спектры поля в области частот первых трех резонансных пиков.

3. Показано, что спектры изменяются в течение суток как целое, что говорит о том, что эти изменения обусловлены вариациями уровня мировой грозовой активности. Получена интегральная оценка суточных изменений уровня мировых гроз.

4. Результаты мониторинга шумановского резонанса явно указывают на наличие трех мировых грозовых центров, один из которых (Африка) регистрируется по компоненте H_x , а два других (Азия и Америка) по компоненте H_y .

5. Получены данные о сезонных изменениях активности в мировых грозовых центрах: времена максимальной активности и относительные величины пиковых значений.

Данная работа выполнена при частичной поддержке по гранту ИНТАС № 96-1991.

Литература

1. Блюх П.В., Николаенко А.П., Филиппов Ю.Ф. Глобальные электромагнитные резонансы в полости Земля-ионосфера. Киев: Наукова думка. – 1977. – 200 с.

2. Беляев Г.Г., А.П. Николаенко, А.В. Швец, А.Ю. Щекотов Наблюдения за движением мировой грозовой активности по анализу трехкомпонентных измерений шумановских резонансов // Радиопизика и электроника – Харьков: Ин-т радиопизики и электроники НАН Украины. – 1999. – 4. – № 1. – С. 63-69.

A.V. SHVETS¹, A.P. NICKOLAENKO¹, A.YU. SCHEKOTOV², G.G. BELYAEV²

¹Usikov Institute for Radiophysics and Electronics, National Academy of Sciences of Ukraine

²Institute of Terrestrial Magnetism Ionosphere and Radio Wave Propagation (IZMIRAN) Russian Academy of Sciences

RECONSTRUCTION OF DISTANCE DISTRIBUTION OF THE GLOBAL LIGHTNING ACTIVITY FROM SCHUMANN RESONANCE BACKGROUND

Abstract. Diurnal variations of the global thunderstorm activity are deduced from experimental records of the Schumann Resonance (SR) average spectra measured at Lekhta, Karelia (34° E, 64° N) and Karimshino, Kamchatka (158° E, 53° N) observatories. Detailed information on the spatial structure of the global thunderstorm activity has been revealed using inversion of the measured SR average spectra. This information on the distance distribution of sources was employed for suppression of the distance dependence in the SR spectra and in this way for correct estimation of the world thunderstorm activity variations.

1. INTRODUCTION

Radio waves in the lower end of ELF band propagating within the Earth-ionosphere wave-guide exhibit very low attenuation. Because of interference between radio waves repeatedly passed the globe circumference the phenomenon known as Schumann Resonances is observed in the spectra of natural electromagnetic emissions. SR are excited by lightning discharges and carry information on both sources and propagation properties within the earth-ionosphere waveguide.

The idea by Williams [1] concerning a global tropical thermometer based on measurements of SR reflecting total world-wide lightning activity and its connection with average tropical surface temperature in the last years enhanced the interest to the SR study.

A problem of correct estimation the total lightning intensity by SR observations is connected with distance determination to sources. The observed natural SR signal morphologically consists of the two components. These are SR background formed by overlapping ELF-atmospherics stemmed from the aggregate of lightning discharges

distributed all over the globe and ELF transients or so-called Q-bursts originating from “super”-discharges. Amplitudes of Q-bursts exceed the background level by a factor of ten, and intervals between them are from ~10 seconds to a few minutes. This circumstance allows to analyse Q-bursts as isolated events. While methods for Q-bursts’ sources locations are well developed based on different modifications of the spectral and wave impedance techniques (see e.g. [2] and references therein), the complexity of the aforementioned problem increases, when SR background signal is employed for determination of the total lightning intensity from the SR measurements because observation from a single station will supply different amplitude for both distinct resonance mode and wide band integrated signal depending on partial distances to active thunderstorm centres.

The widespread approach to this problem is based on the model of three world thunderstorm centres covering continental areas in Africa, and South America, and so-called maritime continent in the South-East Asia resulting from the lightning observations. In the work [3] a wide band integrated SR sig-

nal was applied for estimating the total lightning activity to diminish a distance dependence.

As distinct from the mentioned above analyses of the SR background based on preliminary assumptions about spatial lightning distribution a technique for reconstruction of the distance profile of the world-wide lightning intensity has been proposed by Shvets [4]. The approach employs the model of the ELF propagation within the spherically-symmetrical earth-ionosphere cavity, along with the hypothesis about statistical independence of the moments between lightning discharge occurrences and does not require preliminary knowledge on the spatial structure of the world thunderstorm activity.

2. INVERSE PROBLEM SOLUTION

In accordance with [4] the earth surface is divided into a set of a narrow annular stripes with centre at the point of observation. Every stripe is characterised by distance from an observer and it is adopted that all the lightning discharges occurred within a particular stripe form the same distance signatures in the SR spectra measured at the observation point. A direct problem of formation of the average SR spectra, assuming that a Poisson process describes a succession of the ELF atmospheric at an input of a receiver, for the case of magnetic components received by orthogonal horizontal antennas is formulated as follow [4]:

$$|H_x(\omega)|^2 = \left\langle |Idl_s(\omega)|^2 \right\rangle \cdot \sum_{i=1}^N S_{xi} |h(\omega, D_i)|^2 \quad (1)$$

$$|H_y(\omega)|^2 = \left\langle |Idl_s(\omega)|^2 \right\rangle \cdot \sum_{i=1}^N S_{yi} |h(\omega, D_i)|^2, \quad (2)$$

where $h(\omega, D_i)$ is a frequency response by magnetic component attributed to the i^{th} interval, characterized by distance from an observer D_i , ω is an angular frequency, $\left\langle |Idl_s(\omega)|^2 \right\rangle$ is an average source current moment of lightning discharges, N is a number of discharges happened during an analysis interval. Amplitudes of the horizontal

magnetic field components squared $|H_x(\omega)|^2$ and $|H_y(\omega)|^2$ will depend on azimuths to particular lightning discharges φ_s through the coefficient S_{xi} and S_{yi} :

$$S_{yi} = \sum_{s=1}^{S_i} \cos^2 \varphi_s, \quad S_{xi} = \sum_{s=1}^{S_i} \sin^2 \varphi_s, \quad (3)$$

whereas their sum will be independent of the azimuth distribution of the lightning discharges:

$$\begin{aligned} |H_\varphi(\omega)|^2 &= |H_x(\omega)|^2 + |H_y(\omega)|^2 = \\ &= \left\langle |Idl_s(\omega)|^2 \right\rangle \cdot \sum_{i=1}^N S_i |h(\omega, D_i)|^2 \end{aligned} \quad (4)$$

due to the followed by (3) obvious relation: $S_i = S_{yi} + S_{xi}$, where S_i represents an effective total number of discharges within the i^{th} distance interval.

The inverse problem is solved by decomposition of average power field spectra in a series of linearly independent base functions, representing frequency responses of the Earth - ionosphere cavity on the vertical discharges for a full set of distances and then by finding unknown coefficients through a least square method.

3. DATA ACQUISITION

The SR spectra were measured at two distant from each other observation points: Lekhta, Karelia (34° E, 64° N) and Karimshino, Kamchatka (158° E, 53° N). Two different schemes of SR measurements have been arranged. Both of them include two orthogonal horizontal magnetic antennas of the same design oriented in the east-west (H_x) and south-north (H_y) directions. In addition a vertical electric field component at Lekhta and vertical magnetic component at Karimshino (aimed for receiving probable seismic emissions) are measured. The equipment used at Lekhta includes three-channel analog receiver with notch filters that reject interference from power lines and computer based 12-bit data acquisition system described in details in [5]. As distinct

from the Lekhta's equipment a choice of 24-bit ADC has enabled to increase extremely a dynamic range and, in such a way, to simplify the receiver structure used at Karimshino. Signals after the antenna preamplifiers are fed directly to the multi-channel ADC and then to a computer. Specific parameters such as sampling frequencies were taken into account under the successive data processing.

4. ANALYSIS OF AVERAGE SR SPECTRA

An example of averaged over the whole day of 24 June, 2000 measured at Karimshino SR spectra plotted by points at the lower graph of Fig.1 together with resulted from decomposition corresponding spectra fitted to the experimental ones. Results of inversion into the daily average distance profiles (upper graph) are shown in the upper graph of Fig.1. We can see that the resolved distance profile consists of a number of maxima covered wide distance range from ~4 to ~15 Mm, which can be approximately attributed to the world thunderstorm centres.

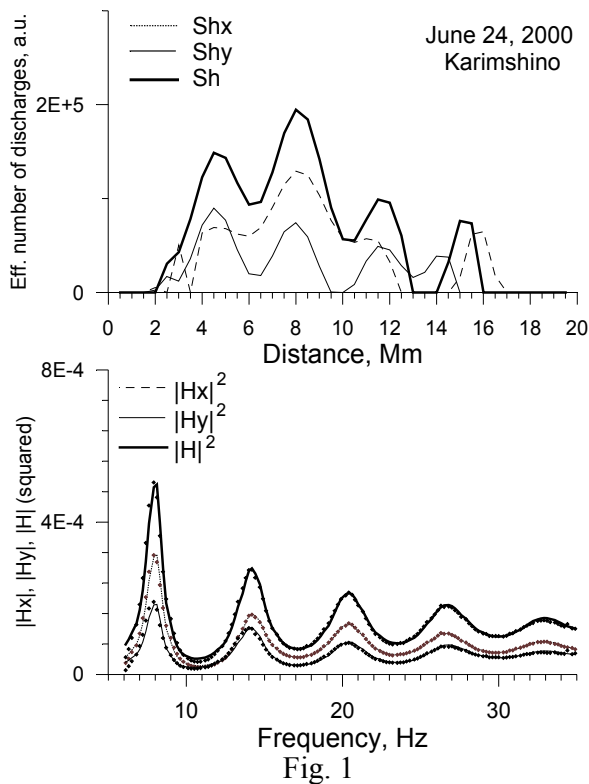


Fig. 1

The receivers are placed essentially different with respect to the world thunderstorm

centres and we expect different distance source distributions observed at these points.

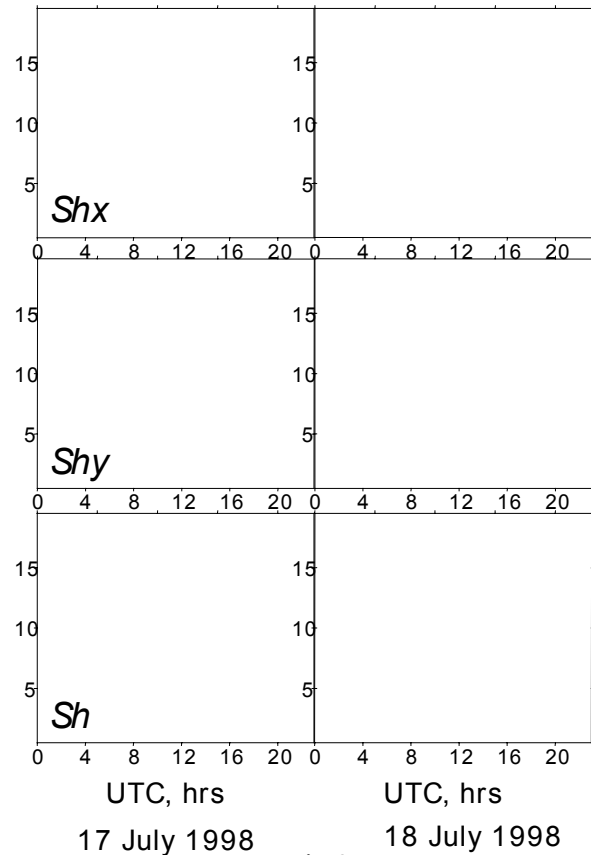


Fig.2.

More compact set of distances is observed from the Lekhta site from which the main active areas are placed mainly in the distance interval from ~6 to ~10 Mm as is seen from contour maps in Fig.2. We can resolve from these maps peculiarities of diurnal spatial redistribution of thunderstorm activity. As was mentioned in [5] the Lekhta site has lucky position with regard to the global thunderstorm centres that enable to observe African sources mainly by H_x component and Asian and American sources by H_y component. This situation is rather clearly can be resolved from the distance profiles reconstructed separately from the magnetic H_x and H_y spectra shown in Fig.2. We can see that during a day the diurnal dependence of the distance profile S_{hy} revealed from the H_x component is represented by a minor (at ~3 h) and major (at ~15 h) maxima appearing at distance of ~7Mm. The profiles S_{hx} recovered from the H_y spectra demonstrate two

maxima occurred at ~8 h and at approximately midnight that can be attributed to Asian (at ~8-9 Mm) and American (at ~9-10 Mm) thunderstorm centres. Composed picture reflecting distance distribution of the

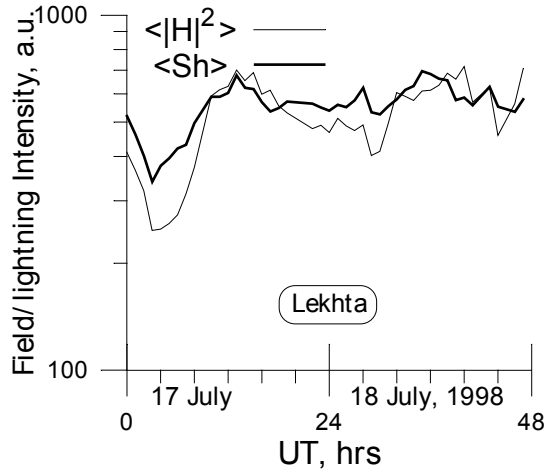


Fig.3.

The graphs presented in Fig.3,4 demonstrate diurnal dependencies of the magnetic field power integrated in the work frequency range 6–35 Hz $\langle |H|^2 \rangle = \langle |H_x|^2 \rangle + \langle |H_y|^2 \rangle$, and integrated over full distance range profiles of the lightning intensities recovered from the full magnetic spectra

$$\langle S_h \rangle = \frac{1}{N} \sum_i S_{hi} \text{ for the Lekhta and}$$

Karimshino observatories respectively. It is observed good correlation between these dependencies. Diurnal variations of the magnetic power reveals higher dynamic range in comparison with reconstructed global lightning intensity.

5. CONCLUSIONS

The technique proposed in [4] is applied for retrieving the total lightning activity variations and its distance profile from measurements of the SR background signal performed at Lekhta (Karelia) and Karimshino (Kamchatka) observatories.

Detailed information on the spatial structure of the global thunderstorm activity has been revealed using inversion of the measured spectra of the SR background signal.

total lightning intensity is observed in the distance profiles S_h recovered from the full horizontal magnetic field.

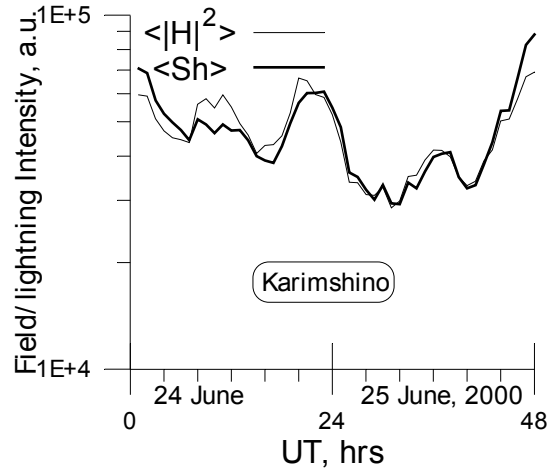


Fig.4.

Results of reconstruction of experimental SR records have shown that the world thunderstorm centres appear as distinct modes in the distance profiles recovered. An additional information about azimuthal distribution of sources was obtained from decomposition of spectra of orthogonal magnetic components. Diurnal redistribution of the lightning activity between the world thunderstorm centres has been demonstrated for the case of the Lekhta observatory.

The information on distance distribution of sources was employed for suppression of the distance dependence in the SR spectra and in this way for correct estimation of the world thunderstorm activity variations. It was found close correlation between diurnal dependencies of the integrated over frequencies power magnetic spectra and total lightning intensity deduced from the SR background signal. Discrepancies do not exceed ~30% during a day that is in accordance with estimations made in [3].

This work was performed in part under support by grant INTAS #1991-96.

References

1. Williams, E. R, The Schumann Resonance: A global tropical thermometer, *Science*, 1992, 256, 1184.

2. Jones D. Ll. ELF spherics and lightning effects on the middle and upper atmosphere, in: Modern Radio Science 1999, Ed. M.A. Stuchly, published for URSI by Oxford Univ. Press, pp. 171-189.
3. Nickolaenko, A.P., G. Satori, B. Zieger, L.M. Rabinowicz, I.G. Kudintseva, Parameters of global thunderstorm activity deduced from the longterm Schumann Resonance records, Journ. Atmos. Solar-Terr. Physics, 1998, 60, 387-399.
4. Shvets A.V. A technique for reconstruction of global lightning distance profile from background Schumann resonance signal, Journ. Atmos. Solar-Terr. Physics, 2001, to be published.
5. Belyaev, G.G., A.Yu. Schekotov, A.V. Shvets, A.P. Nickolaenko, Schumann resonances observed using Poynting vector spectra, Journ. Atmos. Solar-Terr. Physics, 1999, 61, 751-763.

ANDRZEJ W. SOWA RENATA MARKOWSKA

Białystok Technical University, Poland

DYNAMIC BEHAVIOR OF GROUNDING SYSTEMS FOR TELECOMMUNICATION CENTERS

Abstract: Assurance of safe work for people and conditions to correct activities for telecommunication devices require planning and realizations the suitable grounding systems. Taking this fact into account, in article the presentation was made the rules for various calculations of complex grounding systems for telecommunication objects. Special attention was turned on grounding in arrangements tower-telecommunication building with electronic equipment. Grounding was developed adding to basic arrangement - ring earth electrode of tower and ring of building - additional horizontal and vertical earth electrodes. Using proposed numerical methods it was possible to analyse the various grounding systems before their realization and choice optimal solutions.

Proprieties of complex grounding systems were analysed in time and frequency domains using programme TRAGSYS and MALTZ.

1. Introduction

The grounding systems for telecommunication center is design to provide ground references for normal operation of computers nets and telecommunication devices.

Additionally during the lightning stroke or power-supply fault, the grounding systems must be able to cause any danger to persons or damage to insulation or devices.

Therefore design procedures should minimize the maximum values of voltages between different points at the conductors of the grounding systems when surge currents were discharged into the earth.

The behavior of grounding systems excited by surge currents is considerably differs from that at low-frequency currents and the knowledge about the surge resistance is still not at a sufficient level. This problem is very important for telecommunication centers with towers, which are preferential points for lightning strokes.

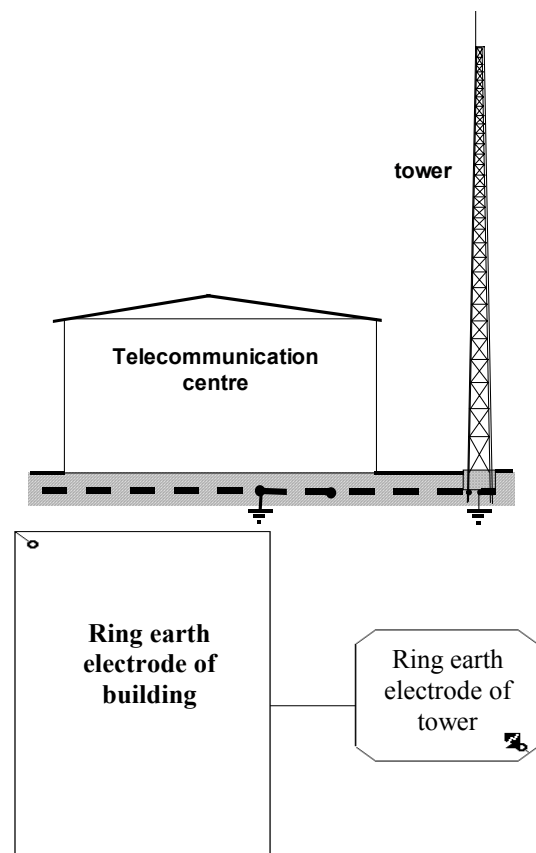


Fig.1. The simplest grounding system of telecommunication centre

The impulse characteristic of these systems are very important to obtained:

- a correct design of surge voltages and currents protection systems in electric installation and signal transmission systems,
- safety and EMC requirements in telecommunication center.

In our calculation we take into account the telecommunication tower, located in the vicinity of a central office building. (Fig.1.) In typical telecommunication center the grounding system consist of a buried rings around the tower and the building.

2. Computational models of the complex grounding systems

Proprieties of complex grounding systems were analysed in time and frequency domains. Grounding impedance was analysed using computer program TRAGSYS [2], which computational algorithm solved numerically complete set of Maxwell's equalizations which described occurrences reaching in grounding systems.

First step in analysis was, in accordance with rules which appeared in methods of moments, partition all grounding system on small segments in ground.

Program TRAGSYS makes possible calculation the grounding in range from 0 Hz to several MHz and defines the surge proprieties during flows of lightning current which have different shapes. Results of calculations were represented in frequency domain and next, after used inverse Fourier's transform, in time domain.

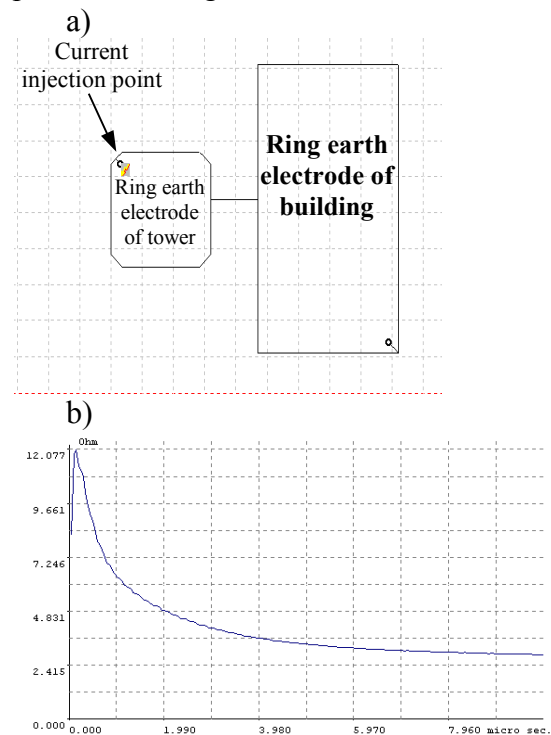
In the purpose of the result's comparison, part of calculation was made using program MALZ [3], which is a part of complex pack of programs CDEGS (Current Distribution Electromagnetic Interference Grounding and Soil Structure Analysis).

3. Grounding systems tower – telecommunication building

We analysed in detail the grounding systems which contained the grounding system of tower and building.

In the case of these objects (fig.1.) the simplest grounding system consists from two simple ring earth electrodes round of tower and building. In our calculation the grounding systems was buried at the depth 0, 8m in the soil with resistivity $100\Omega\text{m}$ and $1000\Omega\text{m}$.

Analyzing proprieties of the grounding systems have been done for currents with different frequencies and for the surge currents which simulated the lightning current. In calculation we used the surge current with amplitude 100 kA and double exponential shape $1/50 \mu\text{s}$. This currents was injected into the tower and lightning protection systems of building. Fig.2. shows the cases when current was injected into the corners of ring earth electrodes of tower (Fig.2a) and building (Fig.2c). The instantaneous surge impedances of grounding systems in these two cases were presented in Fig. 2b and 2d.



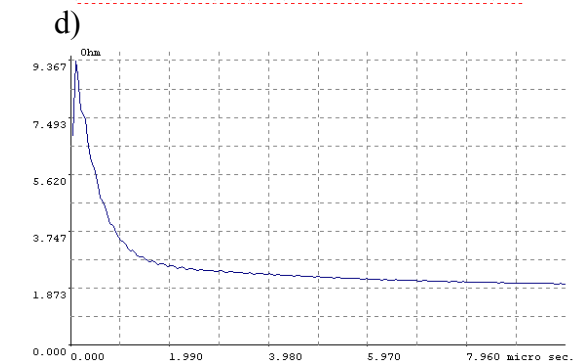
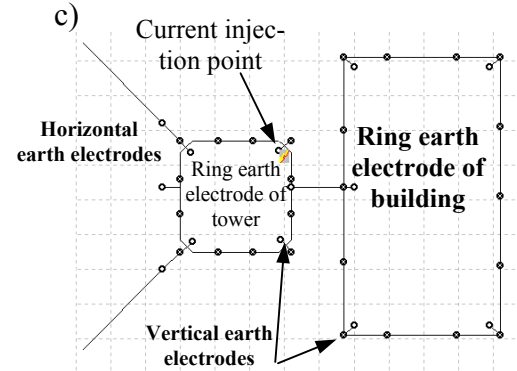
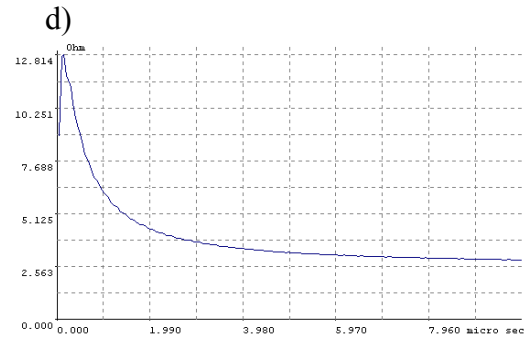
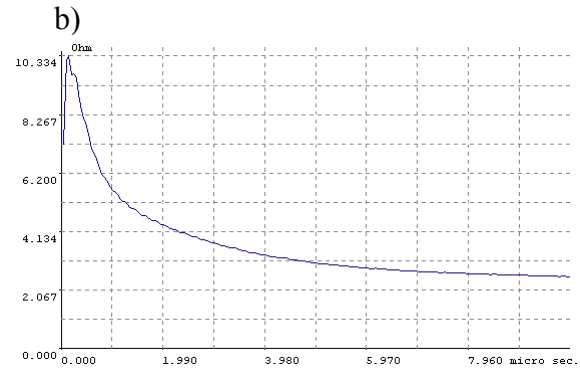
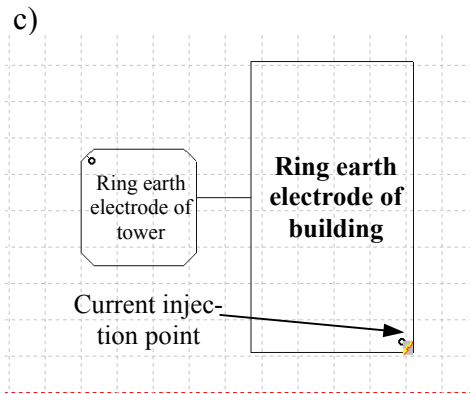


Fig.2. The analysed earth termination systems and the instantaneous surge impedances of these systems.

In such arrangement we examine the static and dynamic properties of ground systems introducing additional:

- vertical earth rod-electrodes about 2, 5m lengths,
- grounding wires between buried rings,
- horizontal earth electrode conductors.

Some examples of analysed grounding systems and surge impedances of earth systems are presented in fig.3.

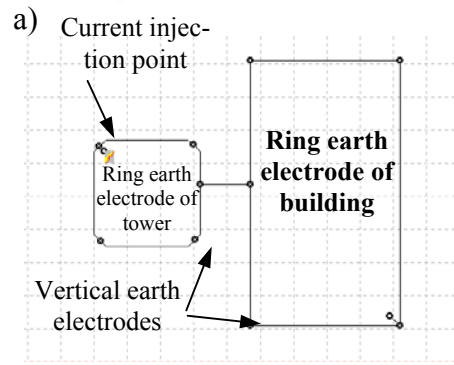


Fig.3. The analysed earth termination systems with additional conductors and the instantaneous surge impedances of these systems.

In calculation we take into account that the horizontal earth electrodes were buried 0,8m deep in soil with resistivity from 100Ωm do 10 000Ωm.

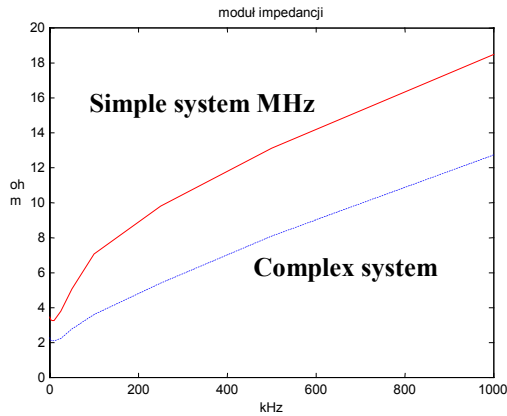
Parametric analysis of the earth systems are carried out:

- at frequencies which changed from 50 Hz to 1 MHz,
- during lightning stroke.

In this last point we determined the surge response of grounding systems. When we analysed the system un frequency domain we computed impedances (modulo and phase) of the earth systems with additional vertical rods (from 4 to 27 rods) in rings. The results are presented in table 1.

Table 1. Impedances of the different earth systems

Arrangement	Modulo	Phase
Simple system – two rings	3,43	-0,30
Simple system with 4 rods in corners of tower's ring	3,26	-0,32
Simple system with 8 rods in corners of tower's and building's rings.	3,08	-0,33
Simple system with 10 rods in corners and in the points of the ring's connection	3,04	-0,34
Simple system with 18 rods.	2,90	-0,36
Simple system with 27 rods	2,70	-0,38



Frequency form 0 to 5 MHz

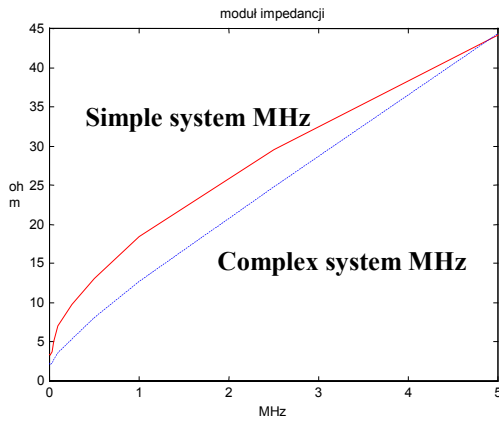
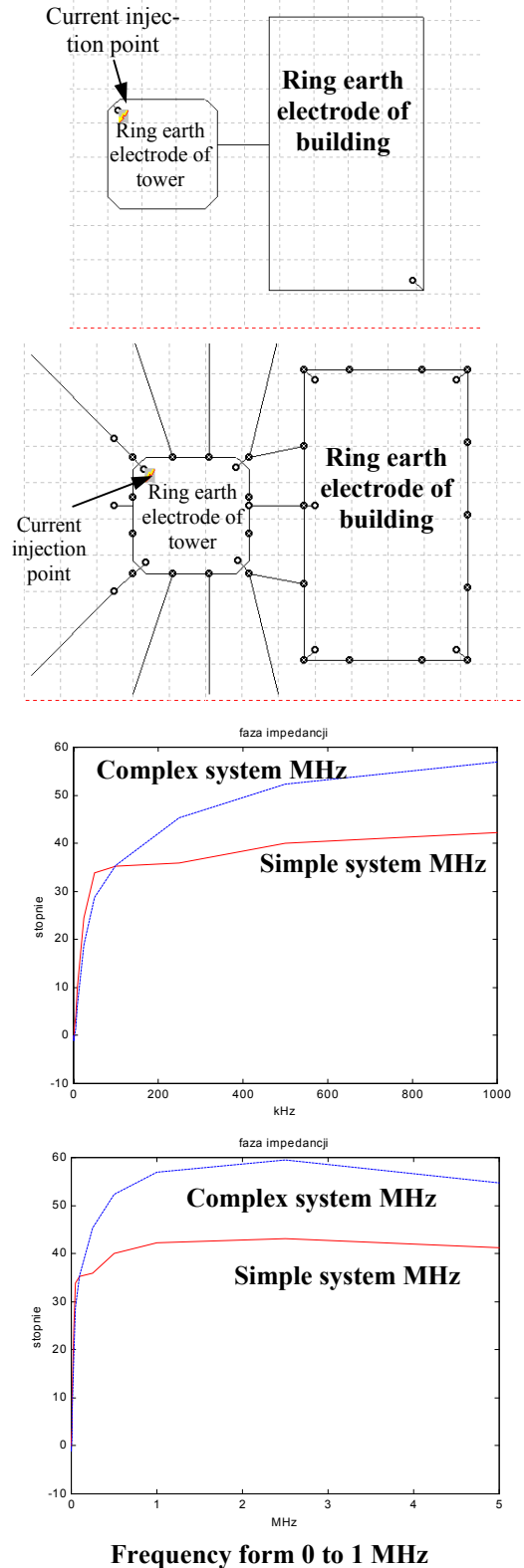


Fig.4. Computed impedances (modulo and phase from 0 to 5 MHz) of simple and complex earth systems

Examples of changes the values of modulo and phases for earth systems impedances in function of frequency (to 5 MHz) are presented in Fig.4.

3. Conclusions

For all earth systems configuration, the simulations are considered with double exponential surge current $1/50 \mu s$ with amplitude 100 kA.



Two different models, based on fields theory and method of moments, were used for high frequency and surge analysis of earth systems.

The surge current was injected in different points of the tower and building's lightning protection systems.

The calculation of earth systems, from simple to complex, shows that the additional vertical and horizontal earth electrodes reduces the values of surge impedance about 25–30 % and the proposed computational method makes seem to be worthwhile for the design the best grounding configuration of telecommunication centers.

References

1. Greew L., Dawalibi F.: An Electromagnetic Model for Transients in Grounding Systems. IEEE Trans. on Power Delivery, vol. PWRD-5, No.4, October 1990, pp.1773-1781.
2. TRAGSYS computer software for Transient Analysis of Grounding Systems – Documentation and Manual.
3. MALZ User's Manual: Frequency Domain Analysis of Buried Conductor Networks" Safe Engineering Services & Technologies Ltd., Montreal Canada

R. MARKOWSKA

Białystok Technical University, Poland

POTENTIAL DISTRIBUTIONS IN GROUNDING SYSTEMS OF TELECOMMUNICATION OBJECTS STRUCK BY LIGHTNING

Abstract: This paper presents the results of computations of voltage distributions in telecommunication grounding systems in case of lightning currents flows. In many cases, the voltage difference between various points of such grounding systems is much convenient value, especially in design, than for example the surge impedance of the system. For that some possible ways of reduction of these transient voltage differences from a point of view of protecting of electronic equipment have been analyzed. Those were mainly the influence of the structure of grounding system and the presence of various additional elements such as vertical ground rods and horizontal conductors. As it is shown in the paper by adding these elements, it is possible to reduce significantly these transient voltages.

1. Introduction

Communication towers are one of the most susceptible structures to direct lightning strikes. Lightning current injected into the tower or building structure should be distributed and drained off possibly uniformly by an appropriate grounding system in order to minimize associated electromagnetic fields and transient voltages to remote ground which can generate high transient voltages in relatively long communication and power line cables and can also be dangerous for personnel. Although it is very important to equalize potential distributions on the whole area of interest, which depends mainly on the surge impedance of the grounding system, in particular cases the analyze of voltage differences between various points of the system may be more useful. These voltage differences

may be somewhat different depending on the structure of the grounding system, even if the surge impedances of various structures are comparable. For example surge impedances of the system from fig. 1b) for various distances between tower and buildings' frames: 9.054Ω for 3m (fig. 2) and 9.045Ω for 7m distance while the voltages obtained for these distances are different (fig. 4a).

Grounding systems analyzed in this paper are typical for buildings associated with communication towers and basically consist of frames surrounding the base of these objects, as shown in fig. 1. The paper presents some results of computations of voltages between extreme grounding points of communication cable (i.e. points 0 and 6 on fig. 1) as well as between grounding points of communication and power line cables at the entry to the building (i.e. point no 0 and any of the points no 1 through 5).

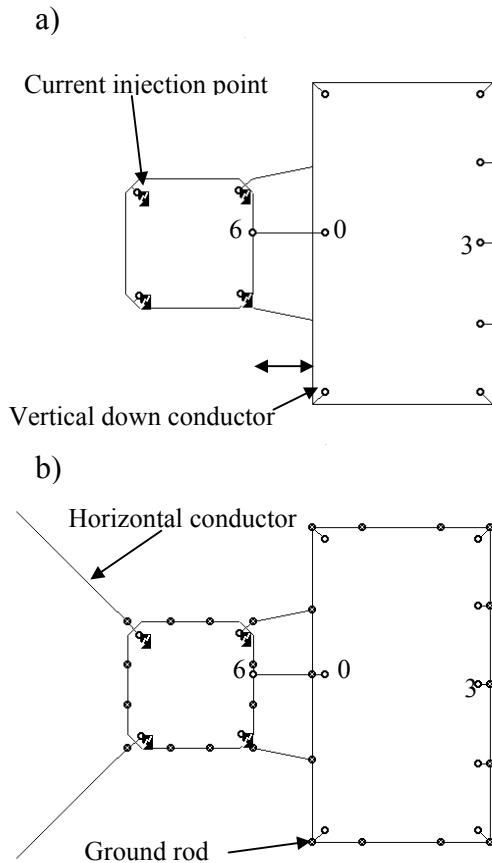


Fig. 1. The analyzed grounding systems of an object consisted of a communication tower and a building; a) simple, b) with additional horizontal conductors and ground rods.

Dimensions of these frames are about 6.4x6.4 m for the tower and 9x16 m for the building. The ground rods are 2.5 m long. All structures are buried at a depth 0.8 m in a soil with resistivity 100Ωm.

Fig. 2 shows instantaneous surge impedance of the system from fig. 1b).

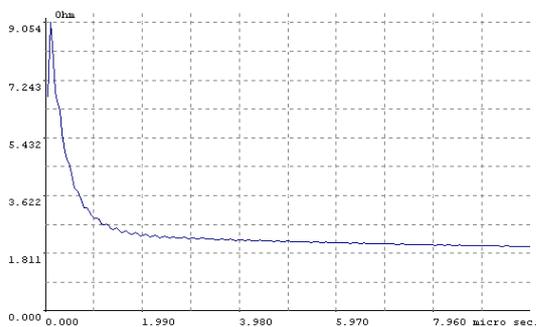


Fig. 2. Surge impedance of the system from fig. 1b)

The computations have been done by means of a computer program, which uses

a rigorous mathematical formulations derived from the complete set of Maxwell's equations, numerically solved by the method of moments [1], [2], [3].

The enargization was simulated by injecting of a current surge of a given shape and amplitude into four points of tower grounding system by means of vertical down conductors. The current surge was chosen as typical lightning of 1/50μs with amplitude 100kA. This current was assumed as distributed uniformly between those points.

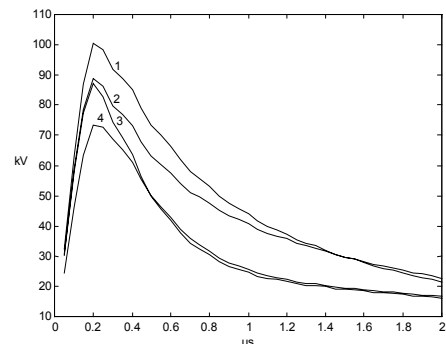
2. Influence of vertical ground rods

Fig. 1a) presents the very simple grounding system, which consists of two frames connected together with 3 horizontal conductors. This simple arrangement was then enlarged step by step, by adding successively: ground rods at the corners of frames, 2 additional horizontal conductors and finally some additional ground rods as shown in fig. 1b).

Fig. 3a) presents in time domain the voltage differences between points 0-6, and fig. 3b) between points 0-1 for these various arrangements. Curve 1 represents the arrangement from fig. 1a), curve 2 – the same structure with additional ground rods at frames' corners, curve 3 – the same as 2 with additional horizontal conductors and finally curve 4 – the arrangement from figure 1b).

It is clear from fig. 2, that the presence of ground rods can significantly reduce these voltages. The reduction is about 27 – 30%.

a)



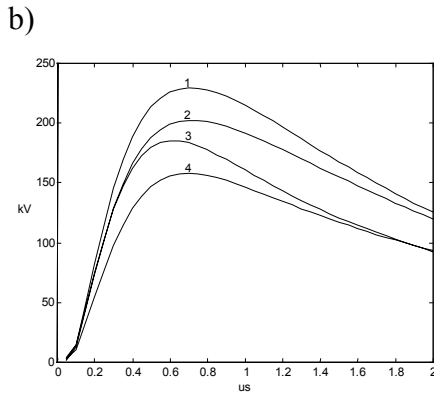


Fig. 3. Time domain voltage differences between points: a) 0-6; b) 0-1; for arrangements: 1 – from fig. 1a); 2 – fig. 1a) with ground rods at frames' corners; 3 – fig. 1a) with ground rods at frames' corners and with two additional horizontal conductors; 4 – fig. 1b).

It has been also estimated that the voltage difference between grounding points of communication and power line cables at the entry to the building does not depend, in fact, on the place of entry of power line cables to the building. Computed voltages between points 0-3, 0-2 or 0-4 are only about 4% greater than that between points 0-1 or 0-5.

3. Connecting tower and buildings' frames

Voltage difference between extreme grounding points of communication cable (i. e. points 0-6) depends, basically, on the distance and the number of connections between tower and building's frames. Fig. 4 presents the time domain transient voltages between these points for the system from fig. 1b) for various distances and number of connections between frames. In case of only 1 connection, it was placed along with the communication cable (directly under the points 0-6). We can see that dependence of voltages on the distance is regular and proportional. For the reduction of this voltage, the distance should be as small as possible. On the other hand, however, it would increase voltage differences on building's grounding system.

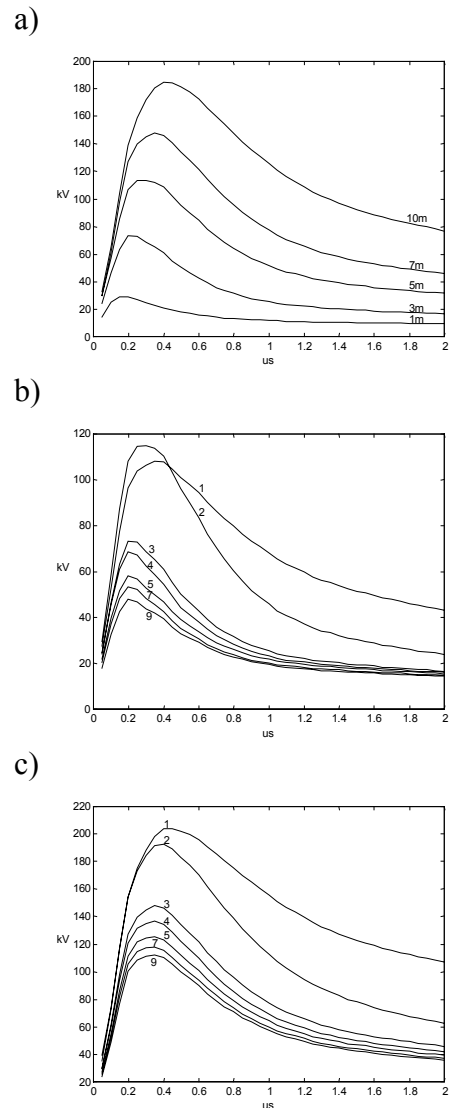


Fig. 4. Time domain voltage difference between points 0-6 of the system from fig. 1b): a) for different distances between tower and building; b) for different number of connections and 3m distance between tower and buildings' frames; c) for different number of connections and 7m distance between tower and buildings' frames.

From fig. 4b) and 4c) it is clear that the frames should be connected together by at least 3 connections with one of them placed close to the communication cable. Increasing number of connections above 3, 4 and greater does not cause such a big change, however the reduction is still significant. Similarly, as in the case of distance, the greater is the number of connections, the larger are voltage differences in building's grounding system. For the arrangement with a 3m distance between

frames, and for 3, 4 or 5 connections, the voltages are about 14% greater in comparison with 2 connections only.

4. Voltages between points on building's grounding system

As it is shown on fig. 3, for the system from fig. 1b), the transient voltages between points 0-1 or 0-5 are over two times greater than between points 0-6. Some additional horizontal conductors have been added to the system from fig. 1b) to reduce these voltages. The analyzed arrangements are shown on fig. 5. The additional conductors are: a) additional frame, surrounding the main building's frame at a distance of 1m, b) additional 3 connections in building's frame, c) both additional frame and 3 connections, d) additional frame together with a grounding grid in building's frame.

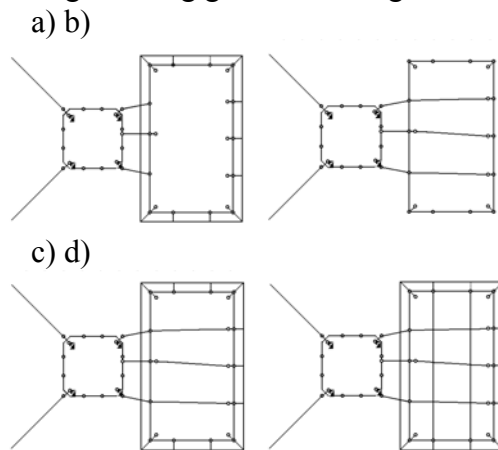


Fig. 5. The analyzed grounding systems with some additional grounding elements. The points between which the computations have been done are marked as in fig. 1.

The resulting transient voltages between points 0-1 and 0-3 for these arrangements are shown on fig. 6. Curves numbered as 1 show the reference voltages obtained in the system from fig. 1b). Significant reduction in voltage difference between points 0-1 and 0-3 for the system from fig. 1 have been obtained by adding 3 connections, as shown on fig. 5b). The reduction is about 27 – 38%.

These improvements have caused increasing of voltage difference along with

the communication cable (between points 0-6) of about 11%.

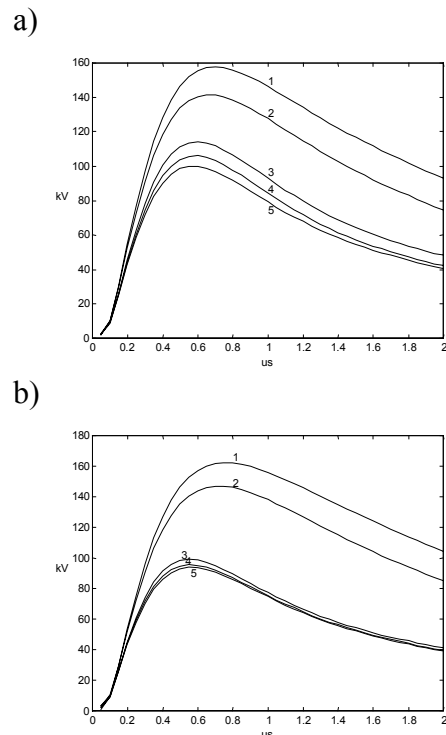


Fig. 6. Time domain voltage differences between points: a) 0-1, b) 0-3; for arrangements: 1 – from fig. 1b), 2 – fig. 5a), 3 – fig. 5b), 4 – fig. 5c), 5 – fig. 5d).

5. Conclusions

In many cases, especially in grounding systems design, the voltage difference between various points of the system is more convenient parameter than the surge impedance, which generally is less susceptible and can not take into consideration all the phenomena. For example, some structures, which differ in some dimensions only can have a comparable surge impedances while the voltages along with that dimensions can differ significantly.

In general, for arrangements such as analyzed in this paper, the main factor that influences the voltage differences between important (from the point of view of protecting of electronic equipment) points of the grounding system is the distance to current injection points. To ensure less voltage difference along with the communication cable, the tower-building distance should be small. However, it can cause relatively large voltage differences between points in building's

grounding system, as it is closer to the current injection point. A similar situation occurs when analyzing the number of connections between tower and buildings' frames. Increasing connections from 2 to 3, 4 or 5 caused increase of voltages in building's grounding system of about 14%.

A significant reduction of voltages between building's grounding systems is possible basically by adding direct connec-

tions that link the opposite flanks of the building's frame (generally a grounding grid). The reduction obtained here was about 30 – 40%, what allowed to maintain these voltages at an amplitude of nearly the same range as for the voltages along with the communication cable, i. e. 100 – 120kV.

The analysis shows that the presence of vertical ground rods in structures plays a significant role in equalization of potentials.

References

1. L. Grcev: Computer analysis of transient voltages in large grounding systems; 1995 IEEE/PES Summer Meeting, Portland, OR, IEEE Paper 95 SM 363-2 PWRD.
2. L. Grcev: Computation of transient voltages near complex grounding systems caused by lightning currents; IEEE 1992 Int. Symp. on EMC, 92CH3169-0, pp. 393–399.
3. L. Grcev, F. Dawalibi: An electromagnetic model for transients in grounding systems; IEEE Transactions on Power Delivery, vol. PWRD-5, no. 4, October 1990, pp.389–399.
4. W. Xiong, F. Dawalibi: Transient performance of substation grounding systems subjected to lightning and similar surge currents; IEEE Transactions on Power Delivery, vol. 9, July 1994, pp. 1421–1427.